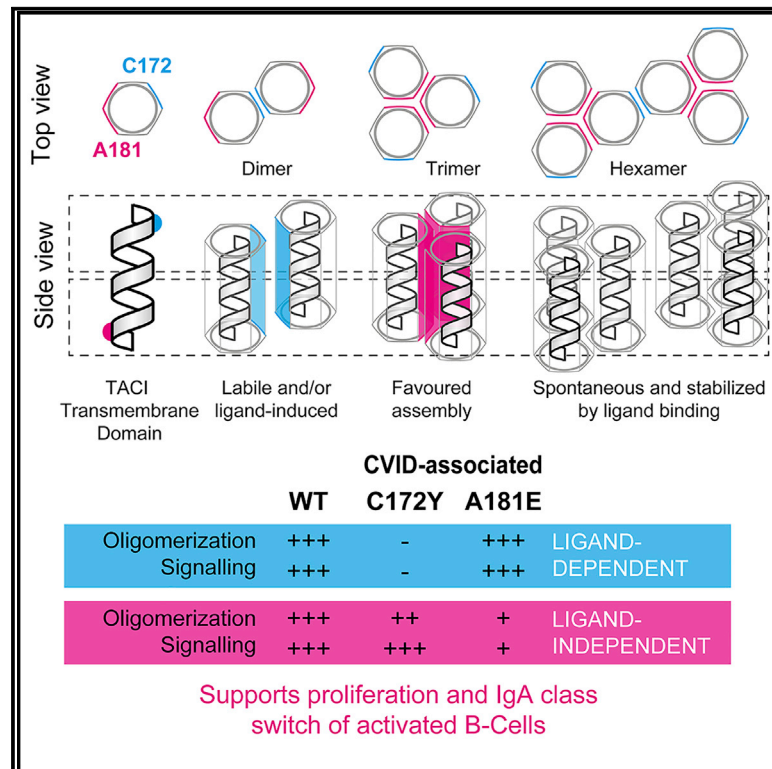


Ligand-independent oligomerization of TACI is controlled by the transmembrane domain and regulates proliferation of activated B cells

Graphical abstract



Authors

Cristian R. Smulski, Luyao Zhang, Malte Burek, ..., Marta Rizzi, Hermann Eibel, Pascal Schneider

Correspondence

pascal.schneider@unil.ch (P.S.), cristian.smulski@cab.cnea.gov.ar (C.R.S.)

In brief

Smulski et al. characterize immunodeficiency-associated mutations in the transmembrane domain of TACI that perturb the complex self-assembly of this receptor, impinging on auto- or ligand-induced signaling. Oligomerization of the transmembrane domain of TACI plays an active role in the proliferation of activated B cells and in antibody production.

Highlights

- TACI transmembrane domain associates via distinct trimeric and dimeric interfaces
- CVID-associated mutation A181E and C172Y affect the trimeric and dimeric interfaces
- TACI transmembrane domain regulates ligand-dependent and -independent signaling
- Spontaneous TACI signals help proliferation and IgA production of activated B cells



Article

Ligand-independent oligomerization of TACI is controlled by the transmembrane domain and regulates proliferation of activated B cells

Cristian R. Smulski,^{1,2,3,*} Luyao Zhang,² Malte Burek,² Ariadna Teixidó Rubio,² Jana-Susann Briem,² Mauricio P. Sica,^{3,4} Eirini Sevdali,² Michele Vigolo,¹ Laure Willen,¹ Patricia Odermatt,² Duygu Istanbulu,² Stephanie Herr,² Marco Cavallari,⁵ Henry Hess,⁶ Marta Rizzi,² Hermann Eibel,^{2,7} and Pascal Schneider^{1,7,8,*}

¹Department of Biochemistry, University of Lausanne, Ch. des Boveresses 155, 1066 Epalinges, Switzerland

²Faculty of Medicine and Medical Center, University of Freiburg, Department of Rheumatology and Center for Chronic Immunodeficiency, Breisacherstr. 115, 79106 Freiburg, Germany

³Medical Physics Department, Centro Atómico Bariloche, Comisión Nacional de Energía Atómica (CNEA), Consejo Nacional de Investigaciones Científicas y Técnicas (CONICET), Avenida E- Bustillo 9500, R8402AGP Río Negro, San Carlos de Bariloche, Argentina

⁴Instituto de Energía y Desarrollo Sustentable, Centro Atómico Bariloche, Comisión Nacional de Energía Atómica (CNEA), Consejo Nacional de Investigaciones Científicas y Técnicas (CONICET), Avenida E- Bustillo 9500, R8402AGP Río Negro, San Carlos de Bariloche, Argentina

⁵BIOSS Centre for Biological Signalling Studies, University of Freiburg, Schänzlestr. 18, 79104 Freiburg, Germany

⁶Merck KGaA, D-64293 Darmstadt, Germany

⁷Senior authors

⁸Lead contact

*Correspondence: pascal.schneider@unil.ch (P.S.), cristian.smulski@cab.cnea.gov.ar (C.R.S.)

<https://doi.org/10.1016/j.celrep.2022.110583>

SUMMARY

In mature B cells, TACI controls class-switch recombination and differentiation into plasma cells during T cell-independent antibody responses. TACI binds the ligands BAFF and APRIL. Approximately 10% of patients with common variable immunodeficiency (CVID) carry TACI mutations, of which A181E and C172Y are in the transmembrane domain. Residues A181 and C172 are located on distinct sides of the transmembrane helix, which is predicted by molecular modeling to spontaneously assemble into trimers and dimers. In human B cells, these mutations impair ligand-dependent (C172Y) and -independent (A181E) TACI multimerization and signaling, as well as TACI-enhanced proliferation and/or IgA production. Genetic inactivation of TACI in primary human B cells impaired survival of CpG-activated cells in the absence of ligand. These results identify the transmembrane region of TACI as an active interface for TACI multimerization in signal transduction, in particular for ligand-independent signals. These functions are perturbed by CVID-associated mutations.

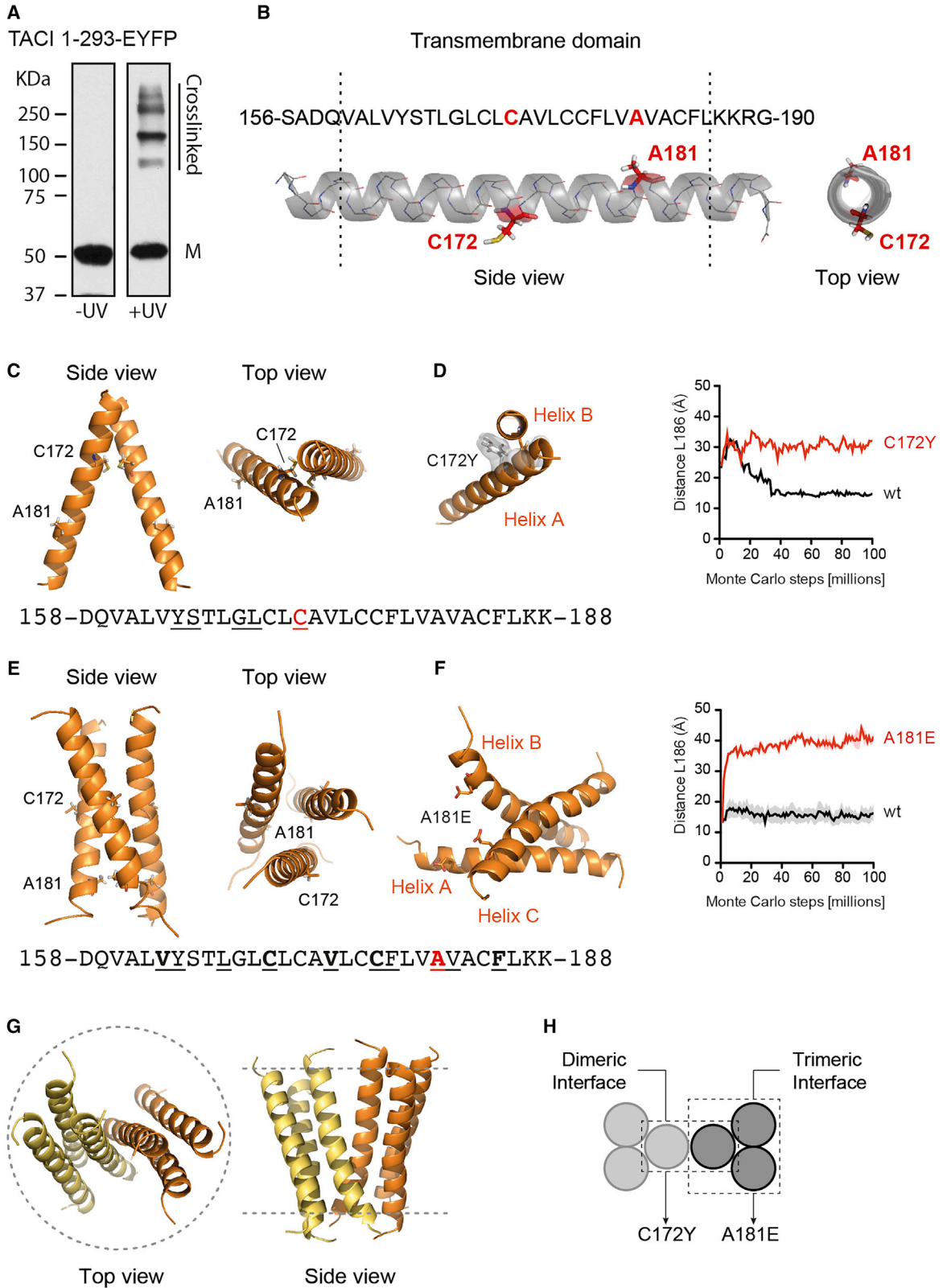
INTRODUCTION

TACI (transmembrane activator and calcium modulator and cyclophilin ligand interactor) is a TNF receptor superfamily member that binds the ligands BAFF (B cell activation factor of the TNF family, BLyS) and APRIL (a proliferation-inducing ligand) (Bodmer et al., 2002; Mackay and Schneider, 2009). In the TNF family, trimeric ligands stimulate membrane-bound receptors, but the form under which receptors respond to ligands is not fully characterized. Receptor dimers, as seen in a crystal structure of TNFR1, or pre-assembled trimers may undergo ligand-induced conformational changes or form multimeric networks when engaged by trimeric ligands to initiate intracellular signaling cascades (Chan et al., 2000; Naismith et al., 1995, 1996). Pre-oligomerization of receptors has also been described for Fas, CD40, TRAILRs (Clancy et al., 2005; Siegel et al., 2000; Smulski et al., 2013, 2017a), and TACI (Garcia-Carmona et al., 2018; Lee et al., 2009). Pre-oligomerization involves the first cysteine-rich domain (CRD) in the extracellular portion of TNFR1, Fas, CD40,

and TRAILRs, while ligand binding is mediated by the second and third CRDs. TACI is a special case as it exists as two splice variants, TACI-L with two CRDs and TACI-S lacking CRD1 (hereafter called TACI Δ CRD1) (Hymowitz et al., 2005). Despite its single CRD, TACI Δ CRD1 can bind its ligands, oligomerize with itself or TACI-L, and support plasma cell development (Garcia-Carmona et al., 2015, 2018). This excludes that TACI oligomerization can be controlled by CRD1 only. TACI Δ CRD1 is thus similar to BAFFR, a receptor whose single CRD appears to promote both oligomerization and BAFF binding (Pieper et al., 2014).

TACI is expressed by activated human B cells, marginal zone B cells, switched memory B cells, and plasma cells. Upon ligand binding, TACI supports T cell-independent type II antibody responses by inducing class-switch recombination and differentiation into plasma cells (Castigli et al., 2005; Salzer et al., 2005). When BAFF binds to TACI and BAFFR, TACI enhances processing of BAFFR by the metalloprotease ADAM10, which limits BAFFR-regulated B cell survival (Smulski et al., 2017b). TACI is





(legend on next page)

also cleaved by ADAM10, releasing a soluble decoy receptor form (sTACI) that can neutralize BAFF and APRIL (Hoffmann et al., 2015). Elevated numbers of B cells in *Taci*^{-/-} mice can be explained by lack of sTACI decoy activity (Bülow von et al., 2001). Also, patients with primary antibody deficiencies harboring TACI mutations affecting expression or ligand binding have elevated BAFF levels and autoimmunity (Kreuzaler et al., 2011; Lee et al., 2009; Salzer et al., 2009). Higher levels of BAFF also correlate with autoimmunity in persons with a mutation that increases the half-life of BAFF mRNA (Steri et al., 2017), a phenotype that is similar to BAFF transgenic mice (Mackay et al., 1999). Thus, by regulating the availability and strength of BAFF-induced survival signals, TACI can control the size of B cell populations. However, switched memory B cells do not depend on BAFF or APRIL for survival, despite expression of both BAFFR and TACI, because they are unaffected or even increased in patients treated with BAFF-neutralizing antibodies or with TACI-Fc (Baker et al., 2020; Stohl et al., 2012; van Vollenhoven et al., 2011; Wallace et al., 2009).

In humans, mutations affecting the structure and function of TACI, such as C104R and A181E, are associated with CVID, the most frequent primary immunodeficiency disorder (Yazdani et al., 2020). Mutation of a single TACI allele is already a risk factor for CVID (Salzer et al., 2009). The TACI C104R mutation disrupts a conserved cysteine residue in CRD2, abolishing ligand binding but not surface expression of TACI (Lee et al., 2009; Salzer et al., 2009). As the C104R variant decreases the decoy activity of sTACI and blunts T-independent B cell responses, CVID patients with this mutation have increased B cell numbers combined with defective T-independent immune responses.

The A181E mutation in the transmembrane (TM) domain of TACI is encoded by the SNP rs72553883, which has an allele frequency of 0.5%–0.6%. The mutation prevents neither surface expression nor ligand binding. Carriers of the A181E mutation have lower levels of anti-pneumococcal polysaccharide IgM and IgG and lower titers of natural anti-*E. coli* antibodies (Castigli et al., 2005; Jabara et al., 2017). The corresponding mutation (A144E) in a transgenic mouse model impaired constitutive and ligand-induced NF- κ B signaling in B cells (Lee et al., 2009). In mice knockin for *Taci* A144E, virtually no TACI was detected and a CVID-like phenotype characterized by severely impaired responses to T-independent antigens and to *S. pneumoniae* infections was observed. In the heterozygous state, TACI expres-

sion was lower than in the wild type (WT) (Jabara et al., 2017). The SNP rs751216929 encoding the variant C172Y in the TM domain has an allele frequency of 0.02% and was also found in CVID patients (Mohammadi et al., 2009). C172Y and A181E have been reported to disturb APRIL-induced activation of NF- κ B and NFAT (Fried et al., 2011).

Structural reports have highlighted an intrinsic role of the TM domains of TNFRs in the formation of dimers (p75NTR) (Nadezhdin et al., 2016), trimers (Fas and TNFR1) (Chou, 2020; Fu et al., 2016), or dimers of trimers (DR5) (Pan et al., 2019). Thus, understanding the structural basis of TM oligomerization may shed light on the mechanism for signal transduction and the impact of disease-associated mutations in this region. Moreover, B cell development and responses of mice carrying the A144E mutation, and of humans carrying the A181E or C172Y variants, differ from those of TACI-deficient mice or C104R carriers, especially for B lymphocytosis and autoimmunity, suggesting that specific activities of TACI may be linked to its TM region. Here, we provide evidence that the TM region of TACI regulates ligand-independent assembly into trimers and to a lesser extent into dimers, to activate NF- κ B and support TLR9-induced proliferation of human B cells. Mutations C172Y and A181E disturbed ligand-dependent as well as ligand-independent functions of TACI, providing a mechanistic explanation for the association of these mutations with primary antibody deficiencies and pointing to a potential ligand-independent role of TACI in regulating B cell homeostasis.

RESULTS

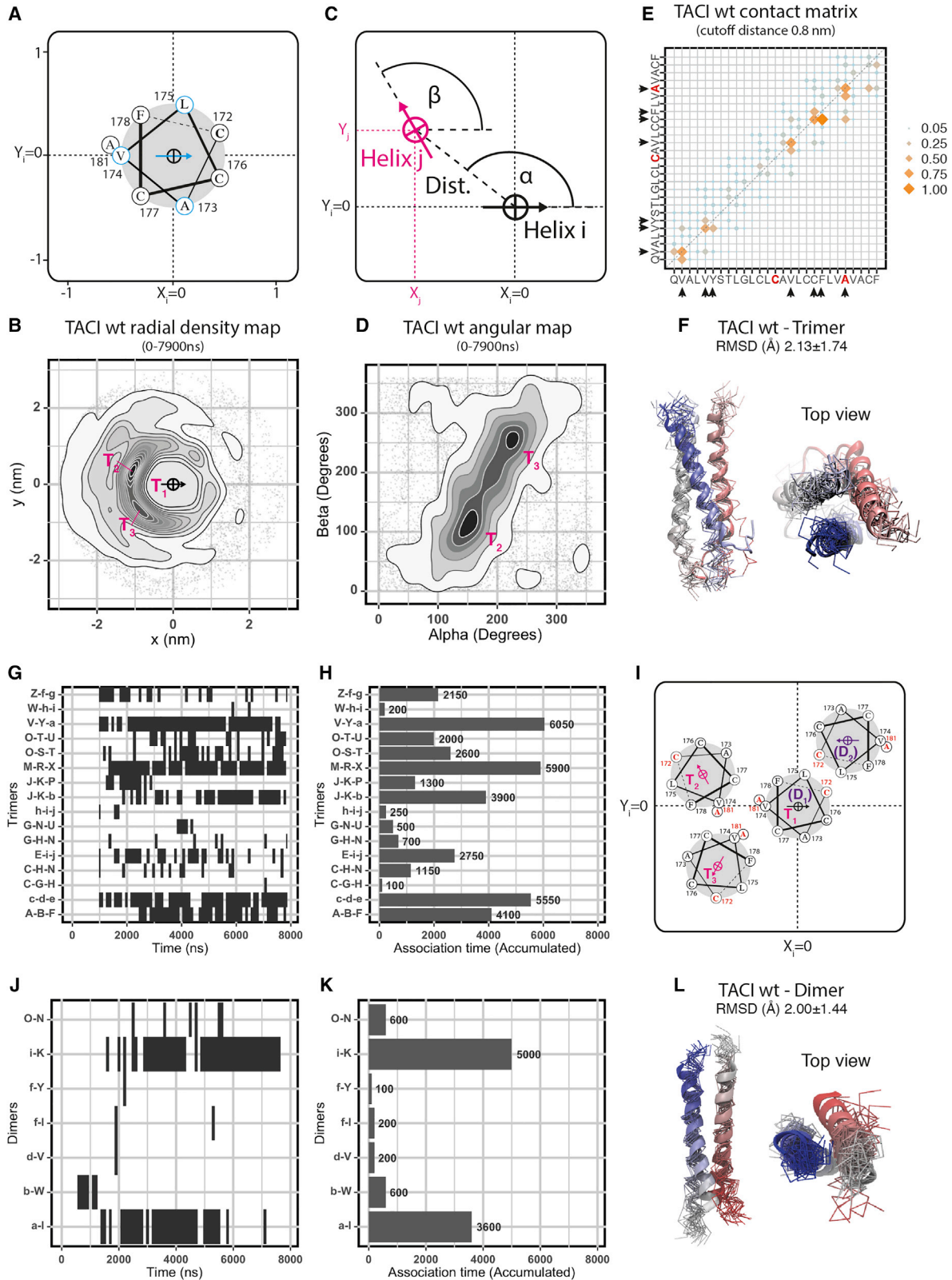
TACI TM assembly model

Evidence that TACI TM self-interacts was first obtained by photo-inducible crosslinking. A TACI-EYFP fusion protein metabolically labeled with a photo-activatable leucine, among others in leucine residues of the TM domain, was specifically crosslinked after a short UV pulse. Crosslinked TACI migrated predominantly as trimers, but also as dimers and higher-order oligomers, possibly hexamers (Figure 1A).

Analysis of the TM helix of TACI showed that residues A181 and C172 point in opposite directions, suggesting they could be part of different association interfaces (Figure 1B). Three programs used to predict dimerization of single-span TM regions, TMDOCK (Lomize and Pogozheva, 2017), PREDDIMER

Figure 1. TACI transmembrane assembly model

- (A) Crosslinking of TACI-EYFP in HEK293T cells labeled with a photo-activatable leucine analog. Whole-cell extracts were analyzed by western blotting using anti-GFP antibodies that recognize EYFP fused to TACI. M, monomer. The image is representative of three independent experiments.
- (B) Side and top views of TACI transmembrane (TM) sequence with C172 and A181 shown in red.
- (C) Model of the dimeric assembly of TACI TM domain that interact through the C172 side obtained using TMDOCK (Lomize and Pogozheva, 2017). Residues involved in helix-to-helix interactions are underlined.
- (D) Mutation C172Y causes a steric hindrance that prevents assembly in a Monte Carlo simulation. The distance between α carbons of leucine 186 along the simulation is shown.
- (E) Trimeric assembly model of TACI based on the structure of Lamp-2A (PDB: 2MOM) facing toward the A181 side. Residues involved in helix-to-helix interactions are underlined. Bold letters indicate residues pointing toward one of the helices in the trimeric unit, underlined plain letters indicate residues pointing to the other helix.
- (F) Mutation A181E induces helix repulsions in a Monte Carlo simulation.
- (G) Structural model of a dimer of trimers of TACI TM domains.
- (H) Scheme of dimeric and trimeric interactions in the TM domain of TACI, and of the predicted impact of C172Y and A181E on these interfaces. See also Figure S1.



(legend on next page)

(Polyansky et al., 2014), and CATM (Mueller et al., 2014) proposed a dimerization interface involving C172 in TAC1 of humans and other mammals (Figures 1C and S1A–S1C). A Monte Carlo simulation with implicit membrane models predicted that mutation C172Y disturbs a closer association of both helices, most probably by steric hindrance caused by the tyrosine residue (Figure 1D).

Modeling of TM regions into trimers requires pre-existing structural information. The TM region of lysosome-associated membrane protein type 2a (LAMP-2a) (Rout et al., 2014), which is 33% identical to TAC1, was selected to model the trimeric assembly of the TAC1 TM domain (Figure 1E). In this model, the A181 residue faces toward the inner side of TAC1 trimers. A Monte Carlo simulation predicted that the trimeric assembly of the TM region is destabilized by the A181E variant (Figure 1F). Monte Carlo simulations of other naturally occurring or rationally designed mutations in the TM region of TAC1 demonstrated anomalies in all cases, but not necessarily with the expected impact on the assembly mode, probably because substitutions also affect protein-lipid interactions that contribute to correct insertion and tilt angle of TM helices in lipid bilayers (Figure S1D).

Thus, crosslinking and modeling studies suggest that the TAC1 TM domain may assemble into dimers and trimers, with residues C172 and A181 participating to dimeric and trimeric interfaces, respectively (Figures 1G and 1H), similar to the published NMR structure of the TM domain of DR5/TRAILR2 that contains both dimeric and trimeric associations in a dimer-trimer network (Pan et al., 2019).

The TAC1 TM domain organizes mainly as trimers through the A181 interface in simulated membranes

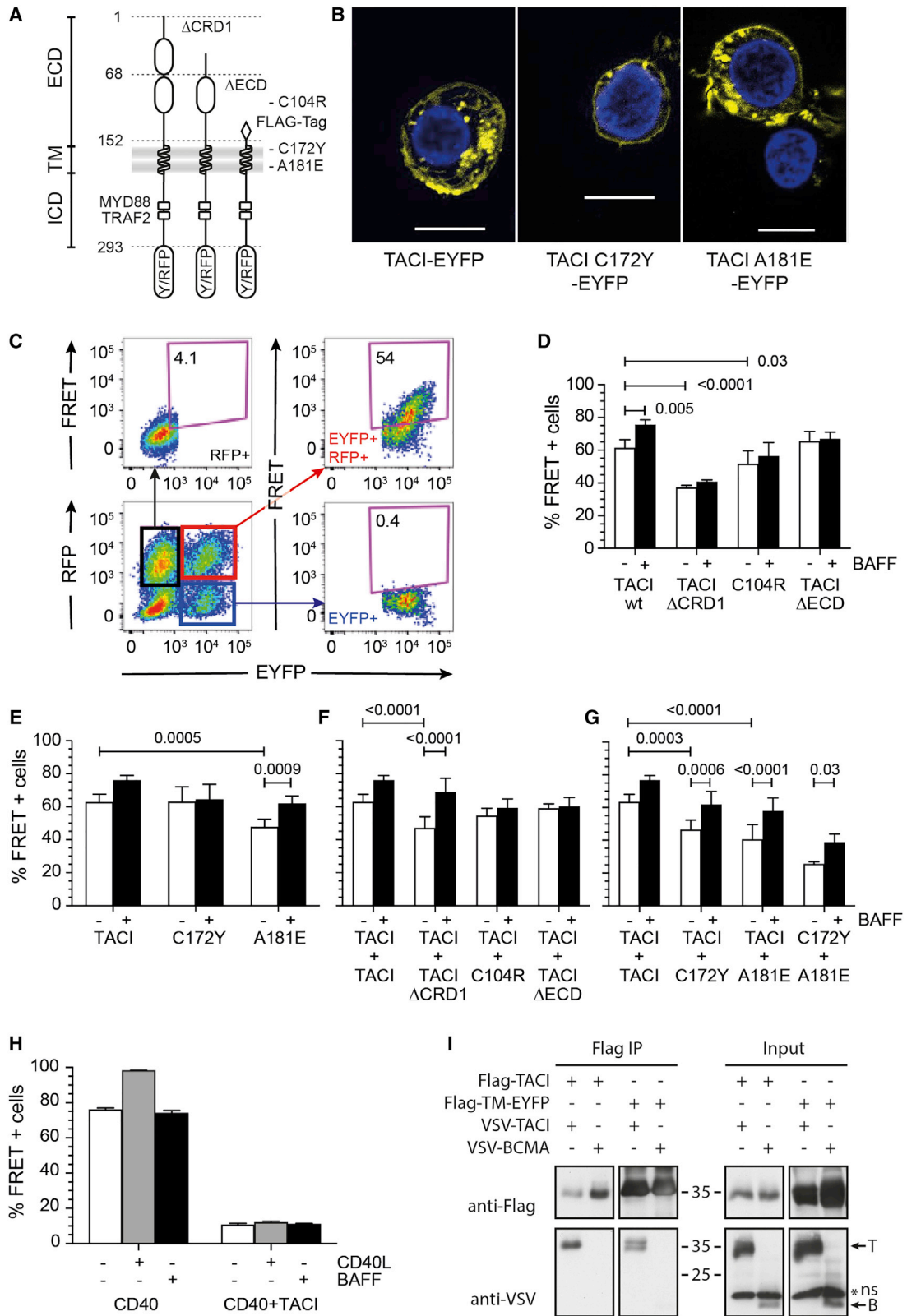
Results of modeling studies were challenged using coarse-grained molecular dynamic simulations. This technique reduces the complexity of a system (proteins, lipids, and water) by treating groups of atoms as “beads” that respect the chemical properties of the molecules, allowing simulations with minimal loss of

structural information but high gain of statistical power. For example, all backbone atoms of an amino acid residue are combined in a backbone bead, while side chains are fitted into additional beads (Marrink et al., 2007; Monticelli et al., 2008; Siewert et al., 2019). Thirty-six copies of TAC1 TM domains (residues 156–190, WT, A181E, or C172Y) were evenly distributed in the x/y plane of a membrane patch of modeled phospholipids and randomly oriented along the z axis (Sica and Smulski, 2021). Their evolution was recorded along 7.9 μ s of simulation (Figure S2A). Three main parameters were recorded: the distance and position at which any helix contacts a reference helix (measured by a distance and by angle α) and the relative orientation of contacting helices (measured by angle β). This was measured repeatedly for each of the 36 helices with a time resolution of 50 ns and cumulated data were plotted into radial density maps (showing the most frequently occupied locations on helices) and angular maps (showing relative orientations of interacting helices) (Figures 2A–2D). Two highly populated spots labeled as T2 and T3 were observed on the A181 side of the reference helix (T1) at α angles of 150° and 220°, respectively (Figure 2B). Beta angles of the interacting helices at positions T2 and T3 were about 120° and 250°, fitting well with predicted angles of 120° and 240° for assembly along a 3-fold symmetry axis (Figure 2D). When all interaction data from 3 to 7.5 μ s were compiled in a contact matrix, residues V160, V163, Y164, V174, C177, F178, and A181 were identified (Figure 2E), which corresponded well to those identified in the trimeric homology model of TAC1 (Figure 1E). Moreover, this model superimposed well with five randomly selected trimers generated in the simulation (root-mean-square deviation of 2.1 ± 1.7 Å) (Figure 2F). Simulation data thus indicate a strong tendency of TAC1 TM helices to assemble as trimers through the A181 side.

The two main spots in the angular map were then extracted using OPTICS clustering, which finds density-based clusters in data of varying density (Ankerst et al., 1999). Three parameters were analyzed: (1) which of the 36 chains were incorporated

Figure 2. The TAC1 TM domain organizes mainly as trimers through the A181 interface in simulated membranes

- (A) Schematic representation of a section of TAC1 TM domain that includes the backbone beads of residues C172 to C176 used to define the centroid of the helix. The orientation vector in cyan was defined as originating from backbone bead V174 and pointing between backbone beads A173 and L175.
- (B) Radial density map of WT TAC1 compiling the density of the xy location of neighboring helices relative to the central one. The map was computed on the full system (36 \times 35) for the complete simulation period (7.9 μ s, sampled every 50 ns) using the centroid of each helix. The denser positions are indicated as T₂ and T₃ (T₁ being the center of the reference helix).
- (C) Diagram depicting α and β angles. In black, a helix chosen as reference in the center of the quadrant (H_i). In magenta, a neighboring helix (H_j) in the x_j/y_j location. The arrows indicate the corresponding orientation vectors.
- (D) Angular map for WT TAC1 showing the preferred relative orientation (β angle) for each position around the central helix defined by the α angle.
- (E) Contact matrix of WT TAC1 at 0.8 nm cutoff distance between backbone beads, performed on the full system (36 \times 35) between 3 and 7.5 μ s. The amino acid sequence corresponds to residues Q159 to F185. Red residues correspond to C172 and A181. The scale corresponds to the number of contacts (NC) normalized to the most frequent one (NC_i/major(NC_j)). Black arrowheads indicate the main residues involved in close interactions.
- (F) Superposition of WT TAC1 trimer model from Figure 1E (cartoon with α helices) with several TAC1 trimers observed during the coarse-grained molecular dynamic simulation (sticks). The root-mean-square deviation (RMSD) of the alignment is shown.
- (G) Unique combination of trimers formed during the simulated period. Data were extracted from the two main clusters in the angular map obtained by OPTICS clustering.
- (H) Accumulated association times for the unique combination of trimers identified in (G).
- (I) Schematic representation of the expected positions in the radial density map (xy plane) for the assembly modes identified in Figure 1. C172 and A181 are indicated in red.
- (J) Same as (G), but for dimers.
- (K) Same as (H), but for dimers.
- (L) Superimposition of WT TAC1 dimer model from Figure 1C (cartoon) with several TAC1 dimers observed during the simulation (sticks). RMSD is indicated. See also Figure S2.



(legend on next page)

within a trimer, (2) with which partners, and (3) how long did these interactions last. In this simulation, 33 out of the 36 helices were incorporated into 16 different and dynamic combinations of trimers, some of which were transient while others lasted for several μs (Figures 2G and 2H).

According to the models in Figure 1C, dimers were expected to be observed with an α angle of 50° and a β angle of $\sim 180^\circ$ (Figure 2I). There was a minor spot at 50° in the radial density map (Figure 2B). This spot was smaller than peaks T1 and T2 because dimers with the “correct orientation” formed less frequently than trimers (2 dimers versus 11 trimers displaying a cumulated association time $>1 \mu\text{s}$); but, then, these dimers could last for several μs just like trimers (Figures 2J and 2K). These stable dimers superimposed well with the dimeric TACI model of Figure 1C (root-mean-square deviation of $2 \pm 1.4 \text{ \AA}$) (Figure 2L).

The analysis of the A181E variant showed an anti-clockwise rotation of the two main spots in the radial density map (α angle) and a rotation of their relative orientations (β angle), suggesting that trimers may still be the preferred assembly mode with differences probably due to repulsion or steric hindrance between glutamic acids (Figures S2B–S2D). Trimer formation in TACI C172Y was also altered to some extent, even though C172 is not directly part of the trimerization interface (Figures S2B–S2D). Dimeric associations were affected in both TACI variants, with a slight distance increase between helices for A181E (1.1 versus 0.9 nm) and a wider distribution of locations and orientations in this region for C172Y. In accord with this simulation data, TACI A181E formed less trimers than WT in UV crosslinking experiments, while TACI C172Y formed less dimers (Figure S2E).

Taken together, these results consolidate the potential of TACI to assemble as a trimer via contacts on the A181 side of the TM helix and, to a lesser extent, as a dimer by contacts on the C172 side. Mutations A181E and C172Y disturb but do not completely abolish these associations.

Oligomerization and interactions of TACI polypeptide chains

To test the extent to which TM domains control TACI interactions in living cells, TACI variants tagged with fluorescent proteins were prepared (Figure 3A). Yellow fluorescent protein (YFP) fused to the intracellular C terminus allowed visualizing membrane expression of TACI WT, A181E, and C172Y expressed by lentiviral gene transfer in BJAB Burkitt’s lymphoma cells (Fig-

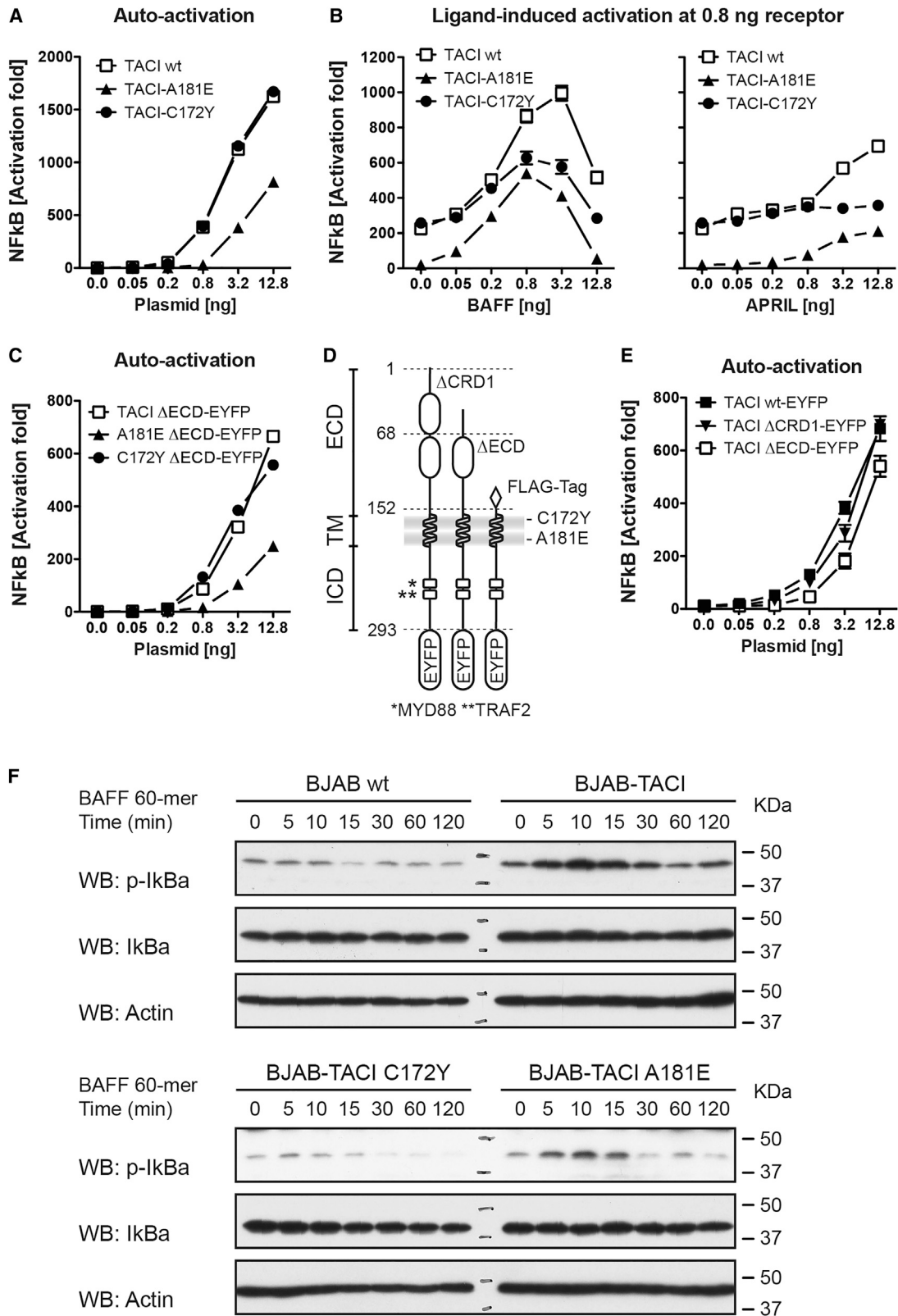
ure 3B). It also allowed detection of Förster resonance energy transfer (FRET) between closely positioned YFP- and RFP-labeled TACI (Figures 3C and 3D). BJAB cells were selected because they express no endogenous TACI. In addition, the chromosomal *BAFFR* alleles were inactivated by CRISPR-Cas9 mutagenesis to suppress interference in BAFF stimulation assays. FRET studies were also performed in transiently transfected HEK293T cells as an independent experimental setting.

Addition of BAFF 60-mers to BJAB cells expressing WT TACI-YFP (amino acid residues 1–293, hereafter called WT TACI) and TACI-RFP further increased FRET+ cells. This ligand-induced increase was consistently seen for all TACI mutants able to bind BAFF when monitored under conventional or heterozygous-like conditions (i.e., when WT and mutant FRET partners were co-expressed). As expected, no ligand-induced increase was observed with TACI C104R that cannot bind BAFF via CRD2 and with TACI lacking the extracellular domain (Flag-TACI 152–293, hereafter called TACI ΔECD). For reasons that remain unclarified, one exception was TACI ΔCRD1 that did not respond to BAFF under conventional conditions (although it did in heterozygous conditions). The other exception was TACI C172Y under conventional conditions, suggesting that C172 directly participates to ligand-induced multimerization and possibly signaling (Figures 3D–3G). In the absence of BAFF, percentages of FRET+ cells were identical for TACI WT and ΔECD in both BJAB and HEK293T cells, underscoring an important role of the TM domain for spontaneous interactions (Figures 3D and S3A). Percentages of FRET+ cells were reduced for TM domain mutations A181E and, to a lesser extent, C172Y, in conventional and heterozygous-like conditions in BJAB and HEK293T cells, except for TACI C172Y in BJAB cells under conventional conditions (Figures 3E, 3G, and S3C–S3G). A contribution of the structural integrity of CRD1 and of CRD2 to TACI associations is suggested by lower percentages of FRET+ cells in BJAB cells expressing TACI ΔCRD1 or TACI C104R. This was, however, not observed in HEK293T cells (Figures 3D and S3A). It is possible that a relatively modest contribution of the extracellular domain to self-association could be masked by higher expression levels in HEK293T cells.

BJAB *BAFFR*-ko cells co-expressing CD40-YFP and -RFP fusion proteins were included as controls for the FRET analyses. The spontaneous association of CD40 was readily detected and further increased after addition of soluble CD40L. CD40 and TACI did not associate so that the percentage of FRET+ cells

Figure 3. Oligomerization and interactions of TACI polypeptide chains

- (A) Cartoon of different TACI variants fused to YFP and RFP.
 (B) Immunofluorescence of TACI-YFP, TACI-C172Y-YFP, and TACI-A181E-YFP expressed in BJAB *BAFFR*-ko cells. Scale bars, 10 μm .
 (C) FACS plots of TACI-YFP and TACI-RFP expressing BJAB cells and the corresponding dot plots displaying the emission of RFP+, YFP+, and YFP+ RFP+ cell populations in the FRET channel. Emission induced by FRET from YFP to RFP fusion proteins of YFP+ RFP+ cells is shown in the upper right panel.
 (D) Percentage of FRET+ cells expressing full-length WT TACI, TACI- ΔCRD1 , TACI-C104R and TACI- ΔECD YFP, and RFP fusions calculated as shown in (C). p values are indicated.
 (E) Same as in (D) but for BJAB cells expressing TACI, C172Y, and A181E fusion proteins. p values are indicated.
 (F) FRET signal induced by co-expressing TACI- ΔCRD1 , TACI-C104R, and TACI- ΔECD -YFP fusion proteins together with WT TACI-RFP. p values are indicated.
 (G) FRET between C172Y- and A181E-YFP fusion proteins and TACI-RFP. Statistically significant differences are shown by the corresponding p values.
 (H) FRET between CD40-YFP/CD40-RFP and CD40-YFP/TACI-RFP \pm BAFF 60-mer or \pm CD40L. All bar graphs represent the mean percentages of FRET+ cells of ≥ 4 independent experiments \pm SD. Signals were first acquired in the absence of BAFF 60-mer, which then was added to a final concentration of 50 ng/mL. After an incubation of 30 min at 37°C , signals were recorded again.
 (I) Co-immunoprecipitation of full-length Flag-tagged TACI, or of the Flag-tagged TM domain of TACI fused to EYFP with full-length VSV-TACI or VSV-BCMA used as negative control. The image of the western blot represents one of two independent experiments. See also Figure S3.



(legend on next page)

remained low and unresponsive to either CD40L or BAFF 60-mer (Figure 3H).

To further support the role of the TM region as a hub for TACI oligomerization, Flag-tagged TACI or Flag-tagged TACI-YFP lacking the extracellular portion and part of the intracellular domain were co-expressed with VSV-tagged TACI and immunoprecipitated using an immobilized anti-Flag antibody. VSV-tagged TACI co-immunoprecipitated with both constructs (Figure 3I), indicating again major contributions of the TM domain and no essential function of the extracellular domain for TACI self-interactions (Figure 3I).

In conclusion, the FRET and co-immunoprecipitation approaches corroborate crosslinking and modeling studies. The ligand-independent oligomerization depends strongly on the TM region, with a possible context-dependent contribution of the extracellular domain. Variants C172Y and A181E in the TM region reduce TACI self-association in BJAB and HEK293T cells. Thus, the dominant phenotype of TACI mutants C104R, A181E, and C172Y in CVID patients (Castigli et al., 2005; Fried et al., 2011; Jabara et al., 2017; Salzer et al., 2005, 2009) could be explained if activation of TACI requires both self-association of the TM domains and ligand binding.

The TACI TM domain regulates ligand-independent and ligand-dependent NF- κ B activation

BAFF binding to TACI enhances clustering (Figure 3) and activates the canonical NF- κ B pathway (Bülow von and Bram, 1997; Xia et al., 2000). As TACI can assemble spontaneously, we tested in HEK293T cells with an NF- κ B luciferase reporter if TACI alone could activate NF- κ B, or in the presence of co-transfected full-length ligands. TACI WT indeed activated NF- κ B in the absence of ligand, and this signal could be further increased by co-transfection of either BAFF or APRIL in conditions where receptor alone did not saturate the response (0.8 ng of plasmid). The trimerization-defective TACI A181E was impaired for ligand-independent signaling, but responded to ligands, while TACI C172Y signaled normally in the absence of ligand, but responded poorly to BAFF and almost not at all to APRIL (Figures 4A and 4B). Similar results were obtained for the AP1 signaling pathway (Figures S4A and S4B). Careful titrations of both TACI and BAFF over wide concentration ranges showed that WT TACI had the strongest ligand-dependent signals at low receptor levels (0.05 ng of plasmid), while TACI A181E required intermediate receptor levels (0.2–0.8 ng of plasmid) for similar effects. TACI C172Y had poor overall responses to

BAFF, suggesting that C172 is involved in transmitting BAFF effects (Figures S4C–S4E).

TACI WT, A181E, and C172Y Δ ECD behaved like the corresponding full-length versions for ligand-independent signaling, although with slightly reduced efficiency (Figures 4C and 4D). Similarly, there was no significant difference in ligand-independent signaling for full-length TACI, TACI Δ CRD1, and TACI Δ ECD, although the latter tended to be less active (Figures 4D and 4E). Unsurprisingly, the intracellular domain was required for signaling. It was unaffected by fusion to a YFP tag, and it was unable to produce any signal when expressed alone without TM domain (Figures S4F–S4H). Together, these results indicate that the intracellular domain of TACI must be multimerized at the plasma membrane via self-association of the TM domain to transmit ligand-independent signals. We do not exclude a contribution of the extracellular domain.

To further evaluate the differential impact of TM TACI mutants in ligand-dependent and -independent signals, mutations A181E and C172Y were combined. The double mutant not only displayed further decreased oligomerization in FRET analysis but was also unable to transmit any ligand-independent or -dependent signals (Figures S5A–S5C). It was, however, expressed normally and, despite reduced surface expression, could bind to both BAFF and APRIL (Figures S5D and S5E).

As phosphorylation of I κ B α by the IKKs is an essential early step in the activation of canonical NF- κ B (Yamamoto and Gaynor, 2004), we tested the impact of mutations A181E or C172Y on TACI-induced phosphorylation of I κ B α . Five minutes after BAFF addition, I κ B α was strongly phosphorylated in BJAB cells expressing WT TACI, then declined within 30 min (Figure 4F). I κ B α was not phosphorylated in cells expressing TACI C172Y, while TACI A181E still allowed I κ B α phosphorylation but less than WT TACI (Figure 4F).

In summary, the C172Y and A181E mutations have distinct effects on TACI signaling. The C172Y mutation, which seems to disturb mainly the dimerization of TACI, did not diminish ligand-independent activation of NF- κ B by TACI but prevented its activation in response to ligand binding. In contrast, the A181E mutation, which was predicted to have a direct impact on trimerization, reduced ligand-independent activation but still allowed ligand-dependent activation of NF- κ B, albeit at a lower extent than WT. Combining both mutations abolished signaling.

Figure 4. TACI TM domain regulates ligand-independent and ligand-dependent activation

- (A) NF- κ B-luciferase reporter assay after transfection of the indicated amounts of plasmids for TACI WT, C172Y, or A181E in the absence of ligand (auto-activation).
 (B) NF- κ B-luciferase reporter assay after transfection of 0.8 ng of TACI WT, A181E, or C172Y with the indicated amounts of BAFF (left) or APRIL (right) plasmid.
 (C) Similar to (A) for the transfection of TACI variants (TACI, A181E, and C172Y) in which the extracellular domain was replaced by a Flag tag (152–293), in the absence of ligand (auto-activation).
 (D) Cartoon of different TACI variants used in the NF- κ B reporter experiments.
 (E) Similar to (A) for the comparison of WT TACI full length, TACI- Δ CRD1 and TACI- Δ ECD, in the absence of ligand (auto-activation). All plasmids have been controlled for similar expression levels at the concentrations used in the experiments. Plots show one representative experiment performed in duplicate out of three independent experiments.
 (F) TACI-negative BJAB cells, and clones of BJAB stably transduced with TACI WT, A181E, and C172Y were incubated with 200 ng/mL of BAFF 60-mer for the indicated time periods. NF- κ B activation was monitored by western blot in whole-cell extracts for I κ B α phosphorylation and degradation. The experiment shown is representative of three independent ones. See also Figures S4 and S5.

Overexpression of TACI enhances proliferation of TLR9-activated B cells

As ligand-independent oligomerization of TACI activated NF- κ B, and because NF- κ B family proteins regulate central steps in B cell activation and proliferation (Gilmore et al., 2004; Kober-Hasslacher et al., 2020; Roy et al., 2019), we reasoned that overexpression of TACI might enhance or even induce proliferation of human B cells. To test this hypothesis, human B cells were transduced with lentiviral expression vectors encoding different TACI-YFP fusion proteins. A signaling-deficient form of TACI-YFP lacking the intracellular TRAF- and Myd88-binding regions (1–223, hereafter called TACI Δ ICD) was used as negative control, while BAFFR-YFP was used as control of a similar receptor with different signaling modalities. To prevent ligand-induced TACI activation, TACI-Fc at 100 ng/mL was added to neutralize BAFF and APRIL potentially produced in the system.

Lentiviral transduction of resting human B cells with a TACI-YFP expression vector did not induce proliferation of YFP-positive cells, but markedly increased CpG- or TLR9-induced proliferation of B cells (Figures 5A, 5B, and S6A). After 4 days of culture, the ratio of proliferating versus resting B cells was, on average, 7.0 ± 1.6 for cells overexpressing TACI-YFP, versus 2.9 ± 1.2 and 1.1 ± 0.3 for TACI Δ ICD-YFP and BAFFR-YFP cells, respectively (Figure 5C). The ratio was intermediate for mutants A181E-YFP (4.0 ± 1.4) and C172Y-YFP (4.4 ± 1.6), but still significantly lower compared with TACI-YFP (Figure 5C). Overexpression of TACI Δ ECD-YFP also enhanced the proliferation significantly above the level observed with TACI Δ ICD-YFP. As TACI Δ ECD assembled with itself and with WT TACI (Figures 3D, 3F, and 3I), and because it activated an NF- κ B luciferase reporter plasmid (Figure 4C), it can be assumed that contacts between the TM regions is required for ligand-independent signaling. However, as the proliferative response of cells overexpressing TACI Δ ECD was weaker than that of WT TACI, interactions between extracellular domains of TACI or between TACI and other proteins, including heparan sulfate proteoglycans, might play a role in regulating proliferation rates. The proliferation rates of cells expressing the ligand binding-deficient mutant C104R were like those of cells expressing WT TACI-YFP, thus supporting the hypothesis that TACI can induce ligand-independent signals to enhance proliferation of TLR9-activated B cells.

CVID patients carrying TACI mutations have typically very low serum IgA titers and very few circulating IgA-positive switched memory B cells (Castigli et al., 2005; Pan-Hammarström et al., 2007; Romberg et al., 2015; Salzer et al., 2005, 2009). Differentiation of naive B cells overexpressing the different forms of TACI into IgA+ plasmablasts in the absence of ligand was observed for cells expressing WT TACI, TACI Δ CRD1, or TACI C104R, and was reduced for TACI A181E but not or less for C172Y (Figure 5D). This suggests that those forms of TACI which oligomerize, like the WT protein, can induce ligand-independent signals, which allowed class-switch recombination of CpG-activated B cells. IgA production was impaired by the TM region mutant A181E, which mainly affected ligand-independent signals in BJAB and HEK293T cells, but not or less by mutant C172Y,

which mainly affected ligand-dependent signals. In TACI Δ ECD, IgA production was impaired, suggesting again a role for the extracellular domain in ligand-independent B cell activation (Figure 5D).

TACI-mediated ligand-independent signals sustain proliferation of CpG-activated primary human B cells

As the expression levels of lentivirally transduced TACI were 10- to 20-fold higher than those of endogenous TACI, the increased proliferation of TACI-expressing B cells might have resulted from clusters of overexpressed TACI molecules. We therefore tested if inactivation of endogenous TACI would reduce proliferation of CpG-activated human B cells.

B cells were electroporated with ribonucleoprotein (RNP) complexes formed from Cas9 and TACI gRNAs (gRNA 5–8), cultured overnight, and activated with CpG, which induced TACI expression in about half of the cells within 3 days (Figure 6A). TACI-Fc was added in the culture medium to block TACI activation by endogenously produced or serum-derived BAFF and/or APRIL. Electroporation with gRNA8/Cas9 RNPs significantly decreased but did not abolish TACI expression, which is not unexpected given that already expressed TACI protein can survive gene inactivation (Figures 6A, 6B, and S6B). This partial reduction of TACI protein levels correlated with lower numbers of cell divisions in TACI-positive cells, while the TACI-negative B cell population, which was less responsive to CpG, was unaffected (Figures 6C–6E). Cells electroporated with gRNA6/Cas9 RNP complexes neither reduced TACI expression nor inhibited CpG-induced B cell proliferation (Figures 6A–6D). The correlation between decreased levels of surface TACI and decreased proliferative response to CpG was statistically significant (Figure S6C). Thus, decreased TACI expression correlated with lower proliferation and/or survival rates, supporting the hypothesis that TACI can modulate the proliferative response of B cells by ligand-independent signaling.

DISCUSSION

Several TNF receptor family members assemble into multimers through interactions of pre-ligand assembly domains (PLAD) that are usually located in the first extracellular cysteine-rich domain (CRD1) (Chan et al., 2000; Clancy et al., 2005; Pieper et al., 2014; Siegel et al., 2000; Smulski et al., 2013). For TACI, other parts of the protein must be involved as TACI Δ CRD1 can still associate with full-length TACI (Garcia-Carmona et al., 2018). The TM domains in different TNFRSF members stabilize homotypic interactions and play active roles in signal transduction (Chou, 2020; Fu et al., 2016; Nadezhdin et al., 2016; Pan et al., 2019), providing a potential explanation for why TACI mutations C172Y and A181E in the TM region disturb downstream functions (Fried et al., 2011; Hammarström et al., 2000; Jabara et al., 2017) and associate with primary antibody deficiencies (Castigli et al., 2005; Fried et al., 2011; Garibyan et al., 2007; Salzer et al., 2005, 2009).

The results of our combined experimental and bioinformatic investigations on TACI TM domain are summarized in a model (Figure S7). Two different sides of the TACI TM domain serve as interfaces for TACI assembly into oligomers. Trimerization through the

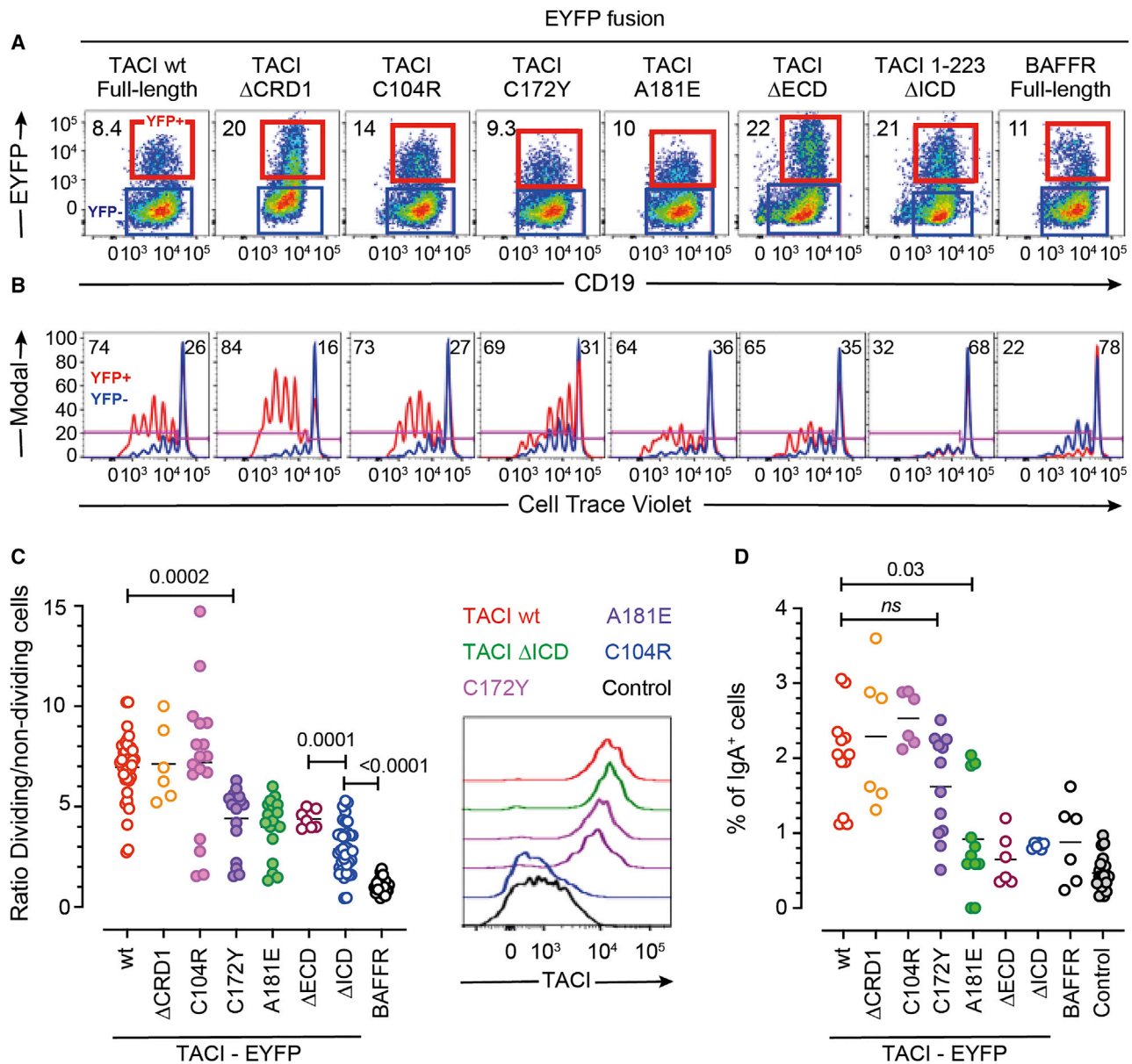


Figure 5. Overexpression of TACI enhances proliferation of TLR9-activated B cells

(A) Human B cells labeled with CellTrace Violet were transduced with lentiviral vectors encoding various TACI-YFP fusion proteins or BAFFR-YFP and activated with 0.1 μ M CpG.

(B) After 5 days of cultivation, proliferation of YFP⁺ or YFP⁻ CD19⁺ cells shown in the red and blue gates, were analyzed by flow cytometry determining the percentage of dividing (CTV⁻) and non-dividing (CTV⁺) cells. Percentages of YFP⁺, CTV⁺, and CTV⁻ cell populations are shown.

(C) Ratio of the percentage of proliferating/non-proliferating YFP⁺ B cells. YFP fusion proteins were made with full-length WT TACI, TACI- Δ CRD1, TACI-C104R, TACI-C172Y, TACI-A181E, TACI- Δ ECD, TACI- Δ ICD, and BAFFR. The insert on the right depicts TACI expression levels of cells expressing YFP fusion proteins and by controls after 4 days of cultivation. p values are indicated.

(D) Percentage of IgA⁺ cells after 4 days of cultivation. p values are indicated. ns: non significant. See also Figure S6A.

side defined by A181 is stable and accounts for most of the observed FRET signals, while dimerization through the side defined by C172 would be induced and/or stabilized by ligands. Indeed, BAFF spontaneously forms 3-mers that can further interact with each other via a loop region called the flap (Vigolo et al., 2018). Flap-flap interactions are too weak to form stable

BAFF 6-mers in solution but may cooperate with weak contacts between C172 dimerization interfaces to form signaling-competent hexameric TACI TM structures. Such hexameric TACI TM structures may also form by “random” associations of TACI trimers via other interfaces at higher TACI concentrations. These alternative interfaces were suggested in the simulation data

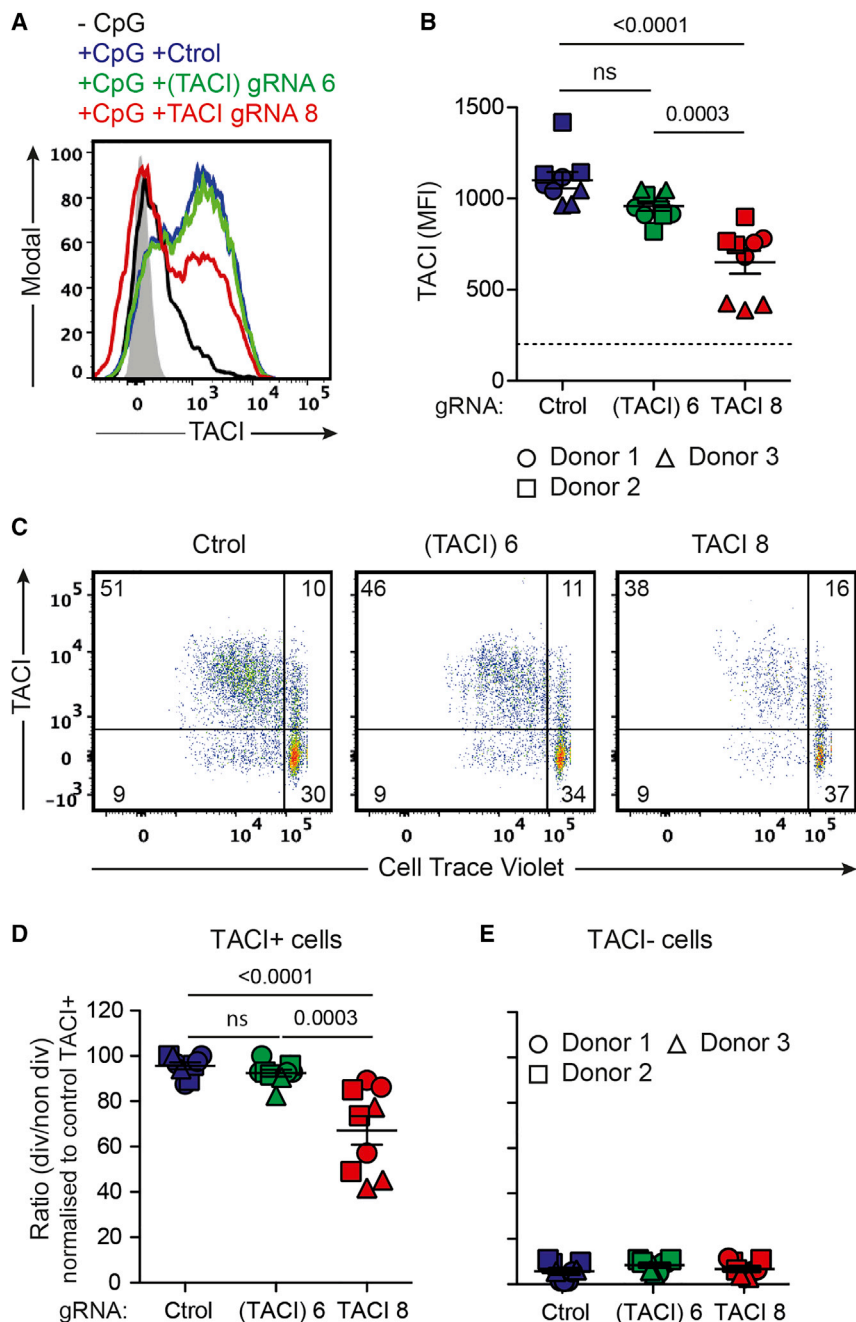


Figure 6. TAC1 ligand-independent signals enhance TLR9-induced proliferation of activated B cells

(A) TAC1 expression visualized by histogram overlays of controls (black) and of B cells activated with 0.1 μ M CpG (blue) for 4 days. To inactivate TAC1, cells were electroporated with TAC1 gRNA 6/Cas9 RTNPs (green) or with TAC1 gRNA 8/Cas9 (red). (B) Mean fluorescence intensity (MFI) of TAC1 on B cells isolated from three different donors electroporated in triplicate with the RNP complexes TAC1 gRNA 6/Cas9 (weakly inactivating) or TAC1 gRNA 8/Cas9 (strongly inactivating), or Cas9 alone (Ctrl), and stimulated for 4 days with 0.1 μ M CpG. The dotted line indicates the MFI of an isotype control. p values are indicated. ns: non-significant. (C) Proliferation of B cells described in (B) detected by the dilution of CellTrace Violet (CTV). (D) Ratio of dividing (CTV low)/non-dividing (CTV high) TAC1-positive B cells normalized to the control condition. This ratio for the control condition was 1.4 for donor 1, 0.7 for donor 2, and 0.2 for donor 3 (circles, squares, and triangles, respectively). p values are indicated. (E) Same as (D) but for TAC1-negative B cells.

mation and signaling in the presence of ligand or stabilize an inactive dimeric state in the absence of ligand.

Overexpression of TAC1 promoted CpG-induced proliferation of primary human B cells as well as the formation of IgA⁺ B cells in the absence of BAFF and APRIL. The C172Y and A181E mutations reduced the proliferation-enhancing activity and A181E also reduced the formation of IgA⁺ cells. Although interactions between the transduced mutant and endogenous WT TAC1 may have masked mutant-specific effects, a fully functional TM domain seems to be required for the formation and/or expansion of IgA⁺ B cells. This stimulatory function of TAC1 could be relevant for the generation of secretory IgA against commensal bacteria in the gut through a T-independent program (Grasset et al., 2020).

In the human population, mutations in the *TAC1* gene occur mainly in the heterozygous state, implying that dimeric or trimeric complexes of TAC1 can consist of

displaying weakly populated spots at angles different from the A181 and C172 interfaces. Mutating hydrophobic A181 to a larger polar residue (A181E) perturbs trimeric interactions making TAC1 less fit to signal. Mutating small polar C172 to a bulky residue (C172Y) would instead impair formation of larger networks of trimers via the C172 interface and decrease response to ligands (Figure S7). Similar to TAC1, the TM domain of DR5/TRAILR2 has distinct dimerization and trimerization faces, allowing formation of dimers of trimers and thus the expansion of an interaction network essential for signal transduction (Pan et al., 2019). PLAD interactions in the extracellular domain may favor hexamer for-

a mix of WT and mutants. With regard to ligand-induced signaling, dominant-negative mutants, such as C104R, would inactivate most of these complexes, while other mutants, such as A181E, would still allow ligand-induced signaling. These differences would explain the incomplete penetrance observed for heterozygous mutations C172Y or A181E (Pan-Hammarström et al., 2007; Salzer et al., 2009), and the dominant-negative role of C104R in primary antibody deficiencies (Garibyan et al., 2007; Romberg et al., 2015). However, none of our results provided sufficient evidence to undoubtedly confirm or exclude such dominant-negative effects. With regard to

ligand-independent signals, activation of NF- κ B measured by a luciferase reporter was unimpaired for TACI C172Y (Figure 4A), yet co-stimulation of CpG-induced proliferation in primary B cells was lower in response to transduced TACI C172Y than WT (Figure 5C). This difference might be explained if signals other than NF- κ B also participate in the proliferative response.

CAML interacts with TACI, at least in yeast two-hybrid experiments (Bülow von and Bram, 1997), raising the question of whether this may involve TM domain interactions. CAML, which has been renamed “guided entry of tail-anchored proteins factor CAMLG,” has been characterized by cryoelectron microscopy as an essential component of a membrane insertion complex for tail-anchored proteins in the endoplasmic reticulum (McDowell et al., 2020). Should CAML interact with the TM domain of TACI (although TACI is not a tail-anchored protein), this may not necessarily be relevant to TACI signaling.

The activation of TLR9 induces TACI expression (Morbach et al., 2016). In turn, co-activation of TACI and TLR9 enhances cell division and differentiation into plasma cells (Chinen et al., 2011; Groom et al., 2007; Martinez-Gallo et al., 2013; Ng et al., 2006; Ozcan et al., 2011; Romberg et al., 2015). Inactivation of TACI in CpG-activated primary B cells reduced TACI expression and impaired cell division. As partial inactivation of TACI impaired CpG-induced proliferation, individual differences in TACI expression might contribute to individual differences in responses to T-independent antigens. Ligand-independent TACI could be especially relevant to T-independent immune responses as TLR7/8- or TLR9-derived signals strongly increase the expression of TACI.

Based on its ligand-independent proliferation-enhancing activity, TACI would fulfill criteria of a proto-oncogene. TACI is elevated in B lymphoma cells (Chiu et al., 2007; Thaler et al., 2017; Yurchenko and Sidorenko, 2010), in gliomas where its level correlates with tumor grade (Pelekanou et al., 2013), and in breast cancer (Kampa et al., 2020). It has been proposed as a new therapeutic target in triple-negative breast cancer (Abo-Elfadl et al., 2020). But, different from typical proto-oncogenes, TACI lacks an enzymatic activity that could be changed by mutations into a constitutive-active receptor. Moreover, TACI is constitutively shed by ADAM10, and the part that remains stuck in the plasma membrane is further processed by γ -secretase (Hoffmann et al., 2015; Meinl et al., 2018). Differently from Notch, which is processed in the same way (Groot and Vooijs, 2012; Radtke et al., 2010), the intracellular part of TACI is degraded. The real oncogenic potential of TACI may thus result from the balance between TACI and ADAM10 levels.

In addition to activated B cells, TACI is constitutively expressed by switched memory B cells and plasma cells, which co-express TACI together with the related receptor BCMA. Survival of naive B cells (Batten et al., 2000; Warnatz et al., 2009) and of plasma cells (O'Connor et al., 2004), but not of switched memory B cells (Benson et al., 2008), depends on BAFF- and/or APRIL-induced pro-survival signals. As switched memory B cells express TACI and BAFFR, but as their survival does not depend on BAFF or APRIL (Furie et al., 2011; van Vollenhoven et al., 2011; Wallace et al., 2009), it would be of interest to determine whether they require TACI, and in particular ligand-independent TACI signals, for their survival and homeostatic proliferation.

In summary we provide evidence that the TM domain of TACI can auto-associate via two distinct interfaces to regulate ligand-dependent and -independent signaling. This association modality can explain the distinct effects of CVID-associated mutations located in this region and provides a model for the ligand-independent activity of TACI in regulating the proliferation of B cells in T-independent immune responses and the homeostasis of switched memory B cells.

STAR★METHODS

Detailed methods are provided in the online version of this paper and include the following:

- KEY RESOURCES TABLE
- RESOURCE AVAILABILITY
 - Lead contact
 - Materials availability
 - Data and code availability
- EXPERIMENTAL MODEL AND SUBJECT DETAILS
 - Cell lines
 - Primary cell cultures
- METHOD DETAILS
 - Immunoprecipitations
 - Luciferase reporter assay
 - Photo-inducible TACI cross-linking
 - Lentiviral gene transfer into primary human B cells
 - Knock out in primary human B cells
 - Molecular modelling
 - Coarse grained molecular dynamic simulations
 - Radial density
 - Contact maps
- QUANTIFICATION AND STATISTICAL ANALYSIS

SUPPLEMENTAL INFORMATION

Supplemental information can be found online at <https://doi.org/10.1016/j.celrep.2022.110583>.

ACKNOWLEDGMENTS

We thank Beate Fischer for excellent technical assistance. This work was supported by grants from the Swiss National Science Foundation (310030_156961 and 31003A_176256 to P.S.), by project funding from Merck KGaA (to P.S.), by the Deutsche Forschungsgemeinschaft (DFG) through P06 of the TRR130 (to H.E.), and by the Hans-Hench-Stiftung and Fondo para la Investigación Científica y Tecnológica (FONCYT) PICT-2018-01107/PICT-2019-00642 (to C.R.S.).

AUTHOR CONTRIBUTIONS

Conceptualization, C.R.S. and P.S.; methodology, C.R.S., M.P.S., M.C., M.R., H.E., and P.S.; investigation, C.R.S., L.Z., M.B., A.T.R., J.-S.B., M.P.S., E.S., M.V., P.O., D.I., S.H., M.C., L.W., H.H., M.R., H.E., and P.S.; writing – original draft, C.R.S. and P.S.; writing – review & editing, C.R.S., H.E., and P.S.; funding acquisition, C.R.S., H.E., and P.S.; resources, M.C., H.H., M.R., H.E., and P.S.; supervision, C.R.S., H.E., and P.S.

DECLARATION OF INTERESTS

H.H. is employee of Merck KGaA. Other authors declare no competing interests.

Received: March 31, 2021
Revised: November 3, 2021
Accepted: March 7, 2022
Published: March 29, 2022

REFERENCES

- Abo-Elfadl, M.T., Gamal-Eldeen, A.M., Ismail, M.F., and Shahin, N.N. (2020). Silencing of the cytokine receptor TNFRSF13B: a new therapeutic target for triple-negative breast cancer. *Cytokine* 125, 154790–154817. <https://doi.org/10.1016/j.cyto.2019.154790>.
- Abraham, M.J., Murtola, T., Schulz, R., Páll, S., Smith, J.C., Hess, B., and Lindahl, E. (2015). GROMACS: high performance molecular simulations through multi-level parallelism from laptops to supercomputers. *SoftwareX* 1-2, 19–25. <https://doi.org/10.1016/j.softx.2015.06.001>.
- Ankerst, M., Breunig, M.M., Kriegel, H.-P., and Sander, J. (1999). OPTICS: ordering points to identify the clustering structure. *ACM SIGMOD Rec.* 28, 49–60. <https://doi.org/10.1145/304181.304187>.
- Baker, D., Pryce, G., James, L.K., Schmierer, K., and Giovannoni, G. (2020). Failed B cell survival factor trials support the importance of memory B cells in multiple sclerosis. *Eur. J. Neurol.* 27, 221–228. <https://doi.org/10.1111/ene.14105>.
- Batten, M., Groom, J., Cachero, T.G., Qian, F., Schneider, P., Tschopp, J., Browning, J.L., and Mackay, F. (2000). BAFF mediates survival of peripheral immature B lymphocytes. *J. Exp. Med.* 192, 1453–1466. <https://doi.org/10.1084/jem.192.10.1453>.
- Benson, M.J., Dillon, S.R., Castigli, E., Geha, R.S., Xu, S., Lam, K.-P., and Noelle, R.J. (2008). Cutting edge: the dependence of plasma cells and independence of memory B cells on BAFF and APRIL. *J. Immunol.* 180, 3655–3659. <https://doi.org/10.4049/jimmunol.180.6.3655>.
- Bodmer, J.L., Schneider, P., and Tschopp, J. (2002). The molecular architecture of the TNF superfamily. *Trends Biochem Sci* 27, 19–26.
- Bülow, von, G.U., and Bram, R.J. (1997). NF-AT activation induced by a CAML-interacting member of the tumor necrosis factor receptor superfamily. *Science* 278, 138–141.
- Bülow, von, G.U., van Deursen, J.M., and Bram, R.J. (2001). Regulation of the T-independent humoral response by TACI. *Immunity* 14, 573–582.
- Bussi, G., Donadio, D., and Parrinello, M. (2007). Canonical sampling through velocity rescaling. *J. Chem. Phys.* 126, 014101. <https://doi.org/10.1063/1.2408420>.
- Castigli, E., Wilson, S.A., Garibyan, L., Rachid, R., Bonilla, F., Schneider, L., and Geha, R.S. (2005). TACI is mutant in common variable immunodeficiency and IgA deficiency. *Nat. Genet.* 37, 829–834. <https://doi.org/10.1038/ng1601>.
- Chan, F.K., Chun, H.J., Zheng, L., Siegel, R.M., Bui, K.L., and Lenardo, M.J. (2000). A domain in TNF receptors that mediates ligand-independent receptor assembly and signaling. *Science* 288, 2351–2354.
- Chinen, J., Martinez-Gallo, M., Gu, W., Cols, M., Cerutti, A., Radigan, L., Zhang, L., Potocki, L., Withers, M., Lupski, J.R., and Cunningham-Rundles, C. (2011). Transmembrane activator and CAML interactor (TACI) haploinsufficiency results in B-cell dysfunction in patients with Smith-Magenis syndrome. *J. Allergy Clin. Immunol.* 127, 1579–1586. <https://doi.org/10.1016/j.jaci.2011.02.046>.
- Chiu, A., Xu, W., He, B., Dillon, S.R., Gross, J.A., Sievers, E., Qiao, X., Santini, P., Hyjek, E., Lee, J.-W., et al. (2007). Hodgkin lymphoma cells express TACI and BCMA receptors and generate survival and proliferation signals in response to BAFF and APRIL. *Blood* 109, 729–739. <https://doi.org/10.1182/blood-2006-04-015958>.
- Chou, J.J. (2020). The Diversity and Similarity of Transmembrane Trimerization of TNF Receptors, fcell-08-569684.tex 1–10. <https://doi.org/10.3389/fcell.2020.569684>.
- Ciancy, L., Mruk, K., Archer, K., Woelfel, M., Mongkolsapaya, J., Screaton, G., Lenardo, M.J., and Chan, F.K.-M. (2005). Pre-ligand assembly domain-mediated ligand-independent association between TRAIL receptor 4 (TR4) and TR2 regulates TRAIL-induced apoptosis. *Proc. Natl. Acad. Sci. U.S.A.* 102, 18099–18104. <https://doi.org/10.1073/pnas.0507329102>.
- Fried, A.J., Rauter, I., Dillon, S.R., Jabara, H.H., and Geha, R.S. (2011). Functional analysis of transmembrane activator and calcium-modulating cyclophilin ligand interactor (TACI) mutations associated with common variable immunodeficiency. *J. Allergy Clin. Immunol.* 128, 226–228.e1. <https://doi.org/10.1016/j.jaci.2011.01.048>.
- Fu, Q., Fu, T.-M., Cruz, A.C., Sengupta, P., Thomas, S.K., Wang, S., Siegel, R.M., Wu, H., and Chou, J.J. (2016). Structural basis and functional role of intramembrane trimerization of the Fas/CD95 death receptor. *Mol. Cell* 61, 602–613. <https://doi.org/10.1016/j.molcel.2016.01.009>.
- Furie, R., Petri, M., Zamani, O., Cervera, R., Wallace, D.J., Tegzová, D., Sanchez-Guerrero, J., Schwarting, A., Merrill, J.T., Chatham, W.W., et al.; BLISS-76 Study Group (2011). A phase III, randomized, placebo-controlled study of belimumab, a monoclonal antibody that inhibits B lymphocyte stimulator, in patients with systemic lupus erythematosus. *Arthritis Rheum.* 63, 3918–3930. <https://doi.org/10.1002/art.30613>.
- García-Carmona, Y., Cols, M., Ting, A.T., Radigan, L., Yuk, F.J., Zhang, L., Cerutti, A., and Cunningham-Rundles, C. (2015). Differential induction of plasma cells by isoforms of human TACI. *Blood* 125, 1749–1758. <https://doi.org/10.1182/blood-2014-05-575845>.
- García-Carmona, Y., Ting, A.T., Radigan, L., Athuluri Divakar, S.K., Chavez, J., Meffre, E., Cerutti, A., and Cunningham-Rundles, C. (2018). TACI isoforms regulate ligand binding and receptor function. *Front Immunol.* 9, 2125. <https://doi.org/10.3389/fimmu.2018.02125>.
- Garibyan, L., Lobito, A.A., Siegel, R.M., Call, M.E., Wucherpfennig, K.W., and Geha, R.S. (2007). Dominant-negative effect of the heterozygous C104R TACI mutation in common variable immunodeficiency (CVID). *J. Clin. Invest.* 117, 1550–1557. <https://doi.org/10.1172/JCI31023>.
- Gilmore, T.D., Kalaitzidis, D., Liang, M.-C., and Starczynowski, D.T. (2004). The c-Rel transcription factor and B-cell proliferation: a deal with the devil. *Oncogene* 23, 2275–2286. <https://doi.org/10.1038/sj.onc.1207410>.
- Grasset, E.K., Chorny, A., Casas-Recasens, S., Gutzeit, C., Bongers, G., Thomsen, I., Chen, L., He, Z., Matthews, D.B., Oropallo, M.A., et al. (2020). Gut T cell-independent IgA responses to commensal bacteria require engagement of the TACI receptor on B cells. *Sci. Immunol.* 5. <https://doi.org/10.1126/sciimmunol.aat7117>.
- Groom, J.R., Fletcher, C.A., Walters, S.N., Grey, S.T., Watt, S.V., Sweet, M.J., Smyth, M.J., Mackay, C.R., and Mackay, F. (2007). BAFF and MyD88 signals promote a lupuslike disease independent of T cells. *J. Exp. Med.* 204, 1959–1971. <https://doi.org/10.1084/jem.20062567>.
- Groot, A.J., and Vooijs, M.A. (2012). The role of Adams in Notch signaling. *Adv. Exp. Med. Biol.* 727, 15–36. https://doi.org/10.1007/978-1-4614-0899-4_2.
- Hammarström, L., Vorechovsky, I., and Webster, D. (2000). Selective IgA deficiency (SIgAD) and common variable immunodeficiency (CVID). *Clin. Exp. Immunol.* 120, 225–231. <https://doi.org/10.1046/j.1365-2249.2000.01131.x>.
- Hoffmann, F.S., Kuhn, P.-H., Laurent, S.A., Hauck, S.M., Berer, K., Wendlinger, S.A., Krumbholz, M., Khademi, M., Olsson, T., Dreyling, M., et al. (2015). The immunoregulator soluble TACI is released by ADAM10 and reflects B cell activation in autoimmunity. *J. Immunol.* 194, 542–552. <https://doi.org/10.4049/jimmunol.1402070>.
- Hymowitz, S.G., Patel, D.R., Wallweber, H.J.A., Runyon, S., Yan, M., Yin, J., Shriver, S.K., Gordon, N.C., Pan, B., Skelton, N.J., et al. (2005). Structures of APRIL-receptor complexes: like BCMA, TACI employs only a single cysteine-rich domain for high affinity ligand binding. *J. Biol. Chem.* 280, 7218–7227. <https://doi.org/10.1074/jbc.M411714200>.
- Jabara, H.H., Lee, J.J., Janssen, E., Ullas, S., Liadaki, K., Garibyan, L., Benson, H., Sannikova, T., Bram, R., Hammarstrom, L., et al. (2017). Heterozygosity for transmembrane activator and calcium modulator ligand interactor A144E causes haploinsufficiency and pneumococcal susceptibility in mice. *J. Allergy Clin. Immunol.* 139, 1293–1301.e4. <https://doi.org/10.1016/j.jaci.2016.07.028>.

- de Jong, D.H., Singh, G., Bennett, W.F.D., Arnarez, C., Wassenaar, T.A., Schäfer, L.V., Periole, X., Tieleman, D.P., and Marrink, S.J. (2013). Improved parameters for the Martini coarse-grained protein force field. *J. Chem. Theor. Comput* 9, 687–697. <https://doi.org/10.1021/ct300646g>.
- Jorgensen, W.L., Maxwell, D.S., and Tirado-Rives, J. (1996). Development and testing of the OPLS all-atom force field on conformational energetics and properties of organic liquids. *J. Am. Chem. Soc. American Chemical Society*. <https://doi.org/10.1021/ja9621760>.
- Kahn, P.C. (2001). Defining the axis of a helix. *Comput. Chem.* 13, 185–189. [https://doi.org/10.1016/0097-8485\(89\)85005-3](https://doi.org/10.1016/0097-8485(89)85005-3).
- Kaminski, G.A., Friesner, R.A., Tirado-Rives, J., and Jorgensen, W.L. (2001). Evaluation and reparametrization of the OPLS-AA force field for proteins via comparison with accurate quantum chemical calculations on peptides. *The J. Phys. Chem. B, American Chemical Society*. <https://doi.org/10.1021/jp003919d>.
- Kampa, M., Notas, G., Stathopoulos, E.N., Tsapis, A., and Castanas, E. (2020). The TNFSF members APRIL and BAFF and their receptors TACI, BCMA, and BAFFR in oncology, with a special Focus in breast cancer. *Front. Oncol.* 10, 827. <https://doi.org/10.3389/fonc.2020.00827>.
- Kienzler, A.-K., Rizzi, M., Reith, M., Nutt, S.L., and Eibel, H. (2013). Inhibition of human B-cell development into plasmablasts by histone deacetylase inhibitor valproic acid. *J. Allergy Clin. Immunol.* 131, 1695–1699. <https://doi.org/10.1016/j.jaci.2013.01.018>.
- Kober-Hasslacher, M., Oh-Strauß, H., Kumar, D., Soberon, V., Diehl, C., Lech, M., Engleitner, T., Katab, E., Fernández-Sáiz, V., Piontek, G., et al. (2020). c-Rel gain in B cells drives germinal center reactions and autoantibody production. *J. Clin. Invest.* 130, 3270–3286. <https://doi.org/10.1172/JCI124382>.
- Kowalczyk-Quintas, C., Willen, D., Willen, L., Golob, M., Schuepbach-Mallepell, S., Peter, B., Eslami, M., Vigolo, M., Broly, H., Samy, E., et al. (2019). No interactions between heparin and atacept, an antagonist of B cell survival cytokines. *Br. J. Pharmacol.* 176, 4019–4033. <https://doi.org/10.1111/bph.14811>.
- Kreuzaler, M., Rauch, M., Salzer, U., Birmelin, J., Rizzi, M., Grimbacher, B., Plebani, A., Lougaris, V., Quinti, I., Thon, V., Litzman, J., Schlesier, M., Warnatz, K., Thiel, J., Rolink, A.G., and Eibel, H. (2011). Soluble BAFF Levels Inversely Correlate with Peripheral B Cell Numbers and the Expression of BAFF Receptors. *J. Immunol.* 188, 497–503. <https://doi.org/10.4049/jimmunol.1102321>.
- Lee, J.J., Rauter, I., Garibyan, L., Ozcan, E., Sannikova, T., Dillon, S.R., Cruz, A.C., Siegel, R.M., Bram, R., Jabara, H., and Geha, R.S. (2009). The murine equivalent of the A181E TACI mutation associated with common variable immunodeficiency severely impairs B-cell function. *Blood* 114, 2254–2262. <https://doi.org/10.1182/blood-2008-11-189720>.
- Lomize, A.L., and Pogozheva, I.D. (2017). TMDOCK: an energy-based method for modeling α -helical dimers in membranes. *J. Mol. Biol.* 429, 390–398. <https://doi.org/10.1016/j.jmb.2016.09.005>.
- Mackay, F., and Schneider, P. (2009). Cracking the BAFF code. *Nat Rev Immunol* 9, 491–502.
- Mackay, F., Woodcock, S.A., Lawton, P., Ambrose, C., Baetscher, M., Schneider, P., Tschopp, J., and Browning, J.L. (1999). Mice transgenic for BAFF develop lymphocytic disorders along with autoimmune manifestations. *J. Exp. Med.* 190, 1697–1710.
- Marrink, S.J., Risselada, H.J., Yefimov, S., Tieleman, D.P., and de Vries, A.H. (2007). The MARTINI force field: coarse grained model for biomolecular simulations. *J. Phys. Chem. B* 111, 7812–7824. <https://doi.org/10.1021/jp071097f>.
- Martinez-Gallo, M., Radigan, L., Almejún, M.B., Martínez-Pomar, N., Matorros, N., and Cunningham-Rundles, C. (2013). TACI mutations and impaired B-cell function in subjects with CVID and healthy heterozygotes. *J. Allergy Clin. Immunol.* 131, 468–476. <https://doi.org/10.1016/j.jaci.2012.10.029>.
- McDowell, M.A., Heimes, M., Fiorentino, F., Mehmood, S., Farkas, Á., Coy-Vergara, J., Wu, D., Bolla, J.R., Schmid, V., Heinze, R., et al. (2020). Structural basis of tail-anchored membrane protein biogenesis by the GET insertase complex. *Mol. Cell* 80, 72–86.e7. <https://doi.org/10.1016/j.molcel.2020.08.012>.
- Meini, E., Thaler, F.S., and Lichtenthaler, S.F. (2018). Shedding of BAFF/APRIL receptors controls B cells. *Trends Immunol.* 39, 673–676. <https://doi.org/10.1016/j.it.2018.07.002>.
- Mohammadi, J., Liu, C., Aghamohammadi, A., Bergbreiter, A., Du, L., Lu, J., Rezaei, N., Amirzargar, A.A., Moin, M., Salzer, U., et al. (2009). Novel mutations in TACI (TNFRSF13B) causing common variable immunodeficiency. *J. Clin. Immunol.* 29, 777–785. <https://doi.org/10.1007/s10875-009-9317-5>.
- Monticelli, L., Kandasamy, S.K., Periole, X., Larson, R.G., Tieleman, D.P., and Marrink, S.-J. (2008). The MARTINI coarse-grained force field: extension to proteins. *J. Chem. Theor. Comput* 4, 819–834. <https://doi.org/10.1021/ct700324x>.
- Morbach, H., Schickel, J.-N., Cunningham-Rundles, C., Conley, M.E., Reisli, I., Franco, J.L., and Meffre, E. (2016). CD19 controls Toll-like receptor 9 responses in human B cells. *J. Allergy Clin. Immunol.* 137, 889–898.e6. <https://doi.org/10.1016/j.jaci.2015.08.040>.
- Mueller, B.K., Subramaniam, S., and Senes, A. (2014). A frequent, GxxxG-mediated, transmembrane association motif is optimized for the formation of interhelical C α -H hydrogen bonds. *Proc. Natl. Acad. Sci. U.S.A.* 111, E888–E895. <https://doi.org/10.1073/pnas.1319944111>.
- Nadezhdin, K.D., García-Carpio, I., Goncharuk, S.A., Mineev, K.S., Arseniev, A.S., and Vilar, M. (2016). Structural basis of p75 transmembrane domain dimerization. *J. Biol. Chem.* 291, 12346–12357. <https://doi.org/10.1074/jbc.M116.723585>.
- Naismith, J.H., Devine, T.Q., Brandhuber, B.J., and Sprang, S.R. (1995). Crystallographic evidence for dimerization of unliganded tumor necrosis factor receptor. *J Biol Chem* 270, 13303–13307.
- Naismith, J.H., Devine, T.Q., Kohno, T., and Sprang, S.R. (1996). Structures of the extracellular domain of the type I tumor necrosis factor receptor. *Structure* 4, 1251–1262.
- Ng, L.G., Ng, C.-H., Woehl, B., Sutherland, A.P.R., Huo, J., Xu, S., Mackay, F., and Lam, K.-P. (2006). BAFF costimulation of Toll-like receptor-activated B-1 cells. *Eur. J. Immunol.* 36, 1837–1846. <https://doi.org/10.1002/eji.200635956>.
- O'Connor, B.P., Raman, V.S., Erickson, L.D., Cook, W.J., Weaver, L.K., Ahoenen, C., Lin, L.-L., Mantchev, G.T., Bram, R.J., and Noelle, R.J. (2004). BCMA is essential for the survival of long-lived bone marrow plasma cells. *J. Exp. Med.* 199, 91–98. <https://doi.org/10.1084/jem.20031330>.
- Ozcan, E., Rauter, I., Garibyan, L., Dillon, S.R., and Geha, R.S. (2011). Toll-like receptor 9, transmembrane activator and calcium-modulating cyclophilin ligand interactor, and CD40 synergize in causing B-cell activation. *J. Allergy Clin. Immunol.* 128, 601–609.e1–4. <https://doi.org/10.1016/j.jaci.2011.04.052>.
- Pan, L., Fu, T.-M., Zhao, W., Zhao, L., Chen, W., Qiu, C., Liu, W., Liu, Z., Piai, A., Fu, Q., et al. (2019). Higher-order clustering of the transmembrane anchor of DR5 drives signaling. *Cell* 176, 1477–1489.e14. <https://doi.org/10.1016/j.cell.2019.02.001>.
- Pan-Hammarström, Q., Salzer, U., Du, L., Björkander, J., Cunningham-Rundles, C., Nelson, D.L., Bacchelli, C., Gaspar, H.B., Offer, S., Behrens, T.W., et al. (2007). Reexamining the role of TACI coding variants in common variable immunodeficiency and selective IgA deficiency. *Nat. Genet.* 39, 429–430. <https://doi.org/10.1038/ng0407-429>.
- Pelekanou, V., Notas, G., Kampa, M., Tsentelieriou, E., Stathopoulos, E.N., Tsapis, A., and Castanas, E. (2013). BAFF, APRIL, TWEAK, BCMA, TACI and Fn14 proteins are related to human glioma tumor grade: immunohistochemistry and public microarray data meta-analysis. *PLoS One* 8, e83250. <https://doi.org/10.1371/journal.pone.0083250>.
- Pieper, K., Rizzi, M., Speletas, M., Smulski, C.R., Sic, H., Kraus, H., Salzer, U., Fiala, G.J., Schamel, W.W., Lougaris, V., et al. (2014). A common single nucleotide polymorphism impairs B-cell activating factor receptor's multimerization, contributing to common variable immunodeficiency. *J. Allergy Clin. Immunol.* 133, 1222–1225. <https://doi.org/10.1016/j.jaci.2013.11.021>.
- Polyansky, A.A., Chugunov, A.O., Volynsky, P.E., Krylov, N.A., Nolde, D.E., and Efremov, R.G. (2014). PREDDIMER: a web server for prediction of

- transmembrane helical dimers. *Bioinformatics* 30, 889–890. <https://doi.org/10.1093/bioinformatics/btt645>.
- Radtke, F., Fasnacht, N., and Macdonald, H.R. (2010). Notch signaling in the immune system. *Immunity* 32, 14–27. <https://doi.org/10.1016/j.immuni.2010.01.004>.
- Romberg, N., Virdee, M., Chamberlain, N., Oe, T., Schickel, J.-N., Perkins, T., Cantaert, T., Rachid, R., Rosengren, S., Palazzo, R., et al. (2015). TNF receptor superfamily member 13b (TNFRSF13B) hemizygoty reveals transmembrane activator and CAML interactor haploinsufficiency at later stages of B-cell development. *J. Allergy Clin. Immunol.* 136, 1315–1325. <https://doi.org/10.1016/j.jaci.2015.05.012>.
- Rout, A.K., Strub, M.-P., Piszczek, G., and Tjandra, N. (2014). Structure of transmembrane domain of lysosome-associated membrane protein type 2a (LAMP-2A) reveals key features for substrate specificity in chaperone-mediated autophagy. *J. Biol. Chem.* 289, 35111–35123. <https://doi.org/10.1074/jbc.M114.609446>.
- Roy, K., Mitchell, S., Liu, Y., Ohta, S., Lin, Y.-S., Metzger, M.O., Nutt, S.L., and Hoffmann, A. (2019). A regulatory circuit controlling the dynamics of NF- κ B cRel transitions B cells from proliferation to plasma cell differentiation. *Immunity* 50, 616–628.e6. <https://doi.org/10.1016/j.immuni.2019.02.004>.
- Salzer, U., Chapel, H.M., Webster, A.D.B., Pan-Hammarström, Q., Schmitt-Graeff, A., Schlesier, M., Peter, H.H., Rockstroh, J.K., Schneider, P., Schäffer, A.A., et al. (2005). Mutations in TNFRSF13B encoding TACI are associated with common variable immunodeficiency in humans. *Nat. Genet.* 37, 820–828. <https://doi.org/10.1038/ng1600>.
- Salzer, U., Bacchelli, C., Buckridge, S., Pan-Hammarström, Q., Jennings, S., Lougaris, V., Bergbreiter, A., Hagen, T., Birmelin, J., Plebani, A., et al. (2009). Relevance of biallelic versus monoallelic TNFRSF13B mutations in distinguishing disease-causing from risk-increasing TNFRSF13B variants in antibody deficiency syndromes. *Blood* 113, 1967–1976. <https://doi.org/10.1182/blood-2008-02-141937>.
- Schneider, P., Willen, L., and Smulski, C.R. (2014). Tools and techniques to study ligand-receptor interactions and receptor activation by TNF superfamily members. *Meth. Enzymol.* 545, 103–125. <https://doi.org/10.1016/B978-0-12-801430-1.00005-6>.
- Sic, H., Kraus, H., Madl, J., Flittner, K.-A., Münchow, von, A.L., Pieper, K., Rizzi, M., Kienzler, A.-K., Ayata, K., Rauer, S., et al. (2014). Sphingosine-1-phosphate receptors control B-cell migration through signaling components associated with primary immunodeficiencies, chronic lymphocytic leukemia, and multiple sclerosis. *J. Allergy Clin. Immunol.* 134, 420–428. <https://doi.org/10.1016/j.jaci.2014.01.037>.
- Sica, M.P., and Smulski, C.R. (2021). Coarse grained molecular dynamic simulations for the study of TNF receptor family members' transmembrane organization. *Front. Cell Dev. Biol.* 8, 11–19. <https://doi.org/10.3389/fcell.2020.577278>.
- Siegel, R.M., Frederiksen, J.K., Zacharias, D.A., Chan, F.K., Johnson, M., Lynch, D., Tsien, R.Y., and Lenardo, M.J. (2000). Fas preassociation required for apoptosis signaling and dominant inhibition by pathogenic mutations. *Science* 288, 2354–2357. <https://doi.org/10.1126/science.288.5475.2354>.
- Siewert, J. Marrink, Corradi, V., Souza, P.C.T., Ingolfsson, H.I., Tieleman, D.P., and Sansom, M.S.P. (2019). Computational Modeling of Realistic Cell Membranes. *Chem Rev.* 119, 6184–6226. <https://doi.org/10.1021/acs.chemrev.8b00460>.
- Smulski, C.R., Beyrath, J., Decossas, M., Chekkat, N., Wolff, P., Estieu-Gionnet, K., Guichard, G., Speiser, D., Schneider, P., and Fournel, S. (2013). Cysteine-rich domain 1 of CD40 mediates receptor self-assembly. *J. Biol. Chem.* 288, 10914–10922. <https://doi.org/10.1074/jbc.M112.427583>.
- Smulski, C.R., Decossas, M., Chekkat, N., Beyrath, J., Willen, L., Guichard, G., Lorenzetti, R., Rizzi, M., Eibel, H., Schneider, P., and Fournel, S. (2017a). Hetero-oligomerization between the TNF receptor superfamily members CD40, Fas and TRAILR2 modulate CD40 signalling. *Cell Death Dis.* 8, e2601. <https://doi.org/10.1038/cddis.2017.22>.
- Smulski, C.R., Kury, P., Seidel, L.M., Staiger, H.S., Edinger, A.K., Willen, L., Seidl, M., Hess, H., Salzer, U., Rolink, A.G., et al. (2017b). BAFF- and TACI-dependent processing of BAFFR by ADAM proteases regulates the survival of B cells. *Cell Rep.* 18, 2189–2202. <https://doi.org/10.1016/j.celrep.2017.02.005>.
- Steri, M., Orrù, V., Idda, M.L., Pitzalis, M., Pala, M., Zara, I., Sidore, C., Faà, V., Floris, M., Deiana, M., et al. (2017). Overexpression of the cytokine BAFF and autoimmunity risk. *N. Engl. J. Med.* 376, 1615–1626. <https://doi.org/10.1056/NEJMoa1610528>.
- Stohl, W., Hiepe, F., Latinis, K.M., Thomas, M., Scheinberg, M.A., Clarke, A., Aranow, C., Wellborne, F.R., Abud-Mendoza, C., Hough, D.R., et al.; BLISS-52 Study Group, BLISS-76 Study Group (2012). Belimumab reduces autoantibodies, normalizes low complement levels, and reduces select B cell populations in patients with systemic lupus erythematosus. *Arthritis Rheum.* 64, 2328–2337. <https://doi.org/10.1002/art.34400>.
- Thaler, F.S., Laurent, S.A., Huber, M., Mulazzani, M., Dreyling, M., Ködel, U., Kümpfel, T., Straube, A., Meinel, E., and Baumgarten von, L. (2017). Soluble TACI and soluble BCMA as biomarkers in primary central nervous system lymphoma. *Neuro Oncol.* 19, 1618–1627. <https://doi.org/10.1093/neuonc/nox097>.
- Ulmschneider, J.P., Ulmschneider, M.B., and Di Nola, A. (2007a). Monte Carlo folding of trans-membrane helical peptides in an implicit generalized Born membrane. *Proteins: Struct. Funct. Bioinformatics* 69, 297–308. <https://doi.org/10.1002/prot.21519>.
- Ulmschneider, M.B., Ulmschneider, J.P., Sansom, M.S.P., and Di Nola, A. (2007b). A generalized born implicit-membrane representation compared to experimental insertion free energies. *Biophysical J.* 92, 2338–2349. <https://doi.org/10.1529/biophysj.106.081810>.
- Vigolo, M., Chambers, M.G., Willen, L., Chevalley, D., Maskos, K., Lammens, A., Tardivel, A., Das, D., Kowalczyk-Quintas, C., Schuepbach-Mallepell, S., et al. (2018). A loop region of BAFF controls B cell survival and regulates recognition by different inhibitors. *Nat. Commun.* 9, 1199. <https://doi.org/10.1038/s41467-018-03323-8>.
- van Vollenhoven, R.F., Kinnman, N., Vincent, E., Wax, S., and Bathon, J. (2011). Atacept in patients with rheumatoid arthritis and an inadequate response to methotrexate: results of a phase II, randomized, placebo-controlled trial. *Arthritis Rheum.* 63, 1782–1792. <https://doi.org/10.1002/art.30372>.
- Wallace, D.J., Stohl, W., Furie, R.A., Lisse, J.R., McKay, J.D., Merrill, J.T., Petri, M.A., Ginzler, E.M., Chatham, W.W., McCune, W.J., et al. (2009). A phase II, randomized, double-blind, placebo-controlled, dose-ranging study of belimumab in patients with active systemic lupus erythematosus. *Arthritis Rheum.* 61, 1168–1178. <https://doi.org/10.1002/art.24699>.
- Warnatz, K., Salzer, U., Rizzi, M., Fischer, B., Gutenberger, S., Böhm, J., Kienzler, A.-K., Pan-Hammarström, Q., Hammarstrom, L., Rakhmanov, M., et al. (2009). B-cell activating factor receptor deficiency is associated with an adult-onset antibody deficiency syndrome in humans. *Proc. Natl. Acad. Sci. U.S.A.* 106, 13945–13950. <https://doi.org/10.1073/pnas.0903543106>.
- Xia, X.Z., Treanor, J., Senaldi, G., Khare, S.D., Boone, T., Kelley, M., Theill, L.E., Colombero, A., Solovyev, I., Lee, F., et al. (2000). TACI is a TRAF-interacting receptor for TALL-1, a tumor necrosis factor family member involved in B cell regulation. *J. Exp. Med.* 192, 137–143.
- Yamamoto, Y., and Gaynor, R.B. (2004). I κ B kinases: key regulators of the NF- κ B pathway. *Trends Biochem. Sci.* 29, 72–79. <https://doi.org/10.1016/j.tibs.2003.12.003>.
- Yazdani, R., Habibi, S., Sharifi, L., Azizi, G., Abolhassani, H., Olbrich, P., and Aghamohammadi, A. (2020). Common variable immunodeficiency: epidemiology, pathogenesis, clinical manifestations, diagnosis, classification, and management. *J. Investig. Allergol. Clin. Immunol.* 30, 14–34. <https://doi.org/10.18176/jiaci.0388>.
- Yurchenko, M., and Sidorenko, S.P. (2010). Hodgkin's lymphoma: the role of cell surface receptors in regulation of tumor cell fate. *Exp. Oncol.* 32, 214–223.

STAR★METHODS

KEY RESOURCES TABLE

REAGENT or RESOURCE	SOURCE	IDENTIFIER
Antibodies		
Mouse anti-CD19 APC/Cy7 (clone HIB19)	Biolegend	Cat# 302218, RRID: AB_314248
Rat anti-TAC1 APC (clone 1A1)	Biolegend	Cat# 311912, RRID: AB_2565423
Goat F(ab') ₂ anti-IgD FITC	SouthernBiotech	Cat# 2032-02, RRID: AB_2687521
Mouse anti-human CD27 PE (clone M-T271)	Biolegend	Cat# 356406, RRID: AB_2561825
Mouse anti-β-actin (clone AC15)	Sigma Aldrich	Cat# A5441, RRID: AB_476744
Anti-GFP antibody	Sigma Aldrich	Cat# 11814460001, RRID:AB_390913
ANTI-FLAG(R) antibody produced in rabbit	Sigma-Aldrich	Cat# F7425, RRID:AB_439687
Mouse Anti-VSV Glycoprotein Monoclonal Antibody, Unconjugated, Clone P5D4	Sigma-Aldrich	Cat# V5507, RRID:AB_261877
Phospho-I B (Ser32) (14D4) Rabbit mAb antibody	Cell Signaling Technology	Cat# 2859, RRID:AB_561111
Mouse Anti-IkappaB-alpha Amino-terminal Antigen Monoclonal Antibody, Unconjugated, Clone L35A5	Cell Signaling Technology	Cat# 4814, RRID:AB_390781
Mouse Anti-TAC1 (ATA1) monoclonal antibody	Merck (Darmstadt, Germany)	250.14.1.1.4.3
Peroxidase-AffiniPure Donkey Anti-Mouse IgG (H+L) antibody	Jackson ImmunoResearch Labs	Cat# 715-035-150, RRID:AB_2340770
Peroxidase-AffiniPure Donkey Anti-Rabbit IgG (H+L) antibody	Jackson ImmunoResearch Labs	Cat# 711-035-152, RRID:AB_10015282
Biotin anti-human CD27 antibody	BioLegend	Cat# 302804, RRID:AB_314296
Chemicals, peptides, and recombinant proteins		
BAFF 60-mer	Produced in house/Adipogen	ps2565/AG-40B-0112-3010
hTAC1 (aa 31–110)-hlgG1 Fc (aa 245–470)	(Kowalczyk-Quintas et al., 2019)	N/A
L-Methionine	Sigma-Aldrich	Cat# 64319
L-Photo-Leucine	Thermo Fisher Scientific	Cat# 22610
Critical commercial assays		
Neon Transfection System 10 μL Kit	Thermo Fischer Scientific	Cat# MPK1096
jetPEI	Polyplus transfection	Cat# 101-10N
NEBuilder HiFi DNA Assembly Cloning Kit	New England Biolabs	Cat# E5520S
PolyFect Transfection Reagent	Qiagen	Cat# 301105
ANTI-FLAG(R) M2 Affinity Gel antibody	Sigma-Aldrich	Cat# A2220, RRID:AB_10063035
MojoSort™ Human Naïve B Cell Isolation Kit	Biolegend	Cat# 480068
Cell Trace Violet	Thermo Fischer Scientific	Cat# C34571
Naive B Cell Isolation Kit II, human	Miltenyi Biotec	Cat# 130-091-150
Experimental models: Cell lines		
BJAB	DSMZ	Cat# ACC-757, RRID:CVCL_5711
HEK293T	DSMZ	Cat# ACC-635, RRID:CVCL_0063

(Continued on next page)

Continued

REAGENT or RESOURCE	SOURCE	IDENTIFIER
Oligonucleotides		
TAC1 gRNA5	Integrated DNA Technologies	Hs.Cas9.TNFRSF13B.1.AA
TAC1 gRNA 6	Integrated DNA Technologies	Hs.Cas9.TNFRSF13B.1.AB
TAC1 gRNA 7	Integrated DNA Technologies	Hs.Cas9.TNFRSF13B.1.AC
TAC1 gRNA 8	Integrated DNA Technologies	Hs.Cas9.TNFRSF13B.1.AL
All sequences are shown in Table S1		N/A
Recombinant DNA		
All plasmids are listed in Table S2		N/A
Software and algorithms		
Flow Jo	https://www.flowjo.com/solutions/flowjo	RRID: SCR_008520
GraphPad Prism	http://www.graphpad.com/	RRID: SCR_002798
Image J	https://imagej.net/	RRID:SCR_003070
GROMACS	http://www.gromacs.org/	RRID:SCR_014565
Pymol	http://www.pymol.org/	RRID:SCR_000305
Hippo	https://www.biowerkzeug.com	N/A
RStudio	http://www.rstudio.com/	RRID:SCR_000432
Deposited data		
Plasmid maps and primary data for all graphs		DOI 10.5281/zenodo.6122280

RESOURCE AVAILABILITY

Lead contact

Further information and requests for resources and reagents should be directed to and will be fulfilled by the lead contact, Pascal Schneider (pascal.schneider@unil.ch).

Materials availability

Plasmids generated in this study are available upon request to the lead contact. Please use the “ps” identification code listed in the plasmid [Table S2](#).

Data and code availability

- Maps of plasmids used in this study and data used for graphs have been deposited on the Zenodo repository, DOI [10.5281/zenodo.6122280](https://doi.org/10.5281/zenodo.6122280). "Zenodo: <https://zenodo.org/record/6122280#.YjOgErgo8II>"
- This paper does not report original code.
- Any additional information required to reanalyze the data reported in this paper is available from the lead contact upon request.

EXPERIMENTAL MODEL AND SUBJECT DETAILS

Cell lines

Human embryonic kidney HEK293T cells were grown in DMEM medium (Gibco) supplemented with 10% foetal calf serum. The human Burkitt lymphoma B cell line BJAB (BAFFR+/TAC1-) was obtained from the DSMZ German Collection of Microorganisms and Cell Cultures and grown in IMDM medium (Gibco) supplemented with 10% foetal calf serum. The identity of BJAB cells was confirmed by microsatellite sequencing (cell line typing service, Microsynth, Balgach, Switzerland). BJAB lines expressing different forms of TAC1, CD40 or BAFF were generated by retroviral and lentiviral transduction with respective expression vectors.

Primary cell cultures

Human B cells were either isolated from the blood of healthy donors or from leucocyte reduction systems and grown in IMDM medium (Gibco) supplemented with 10% foetal calf serum. All experiments with human cells were approved by the Ethics commission of the Albert-Ludwigs-University Freiburg through approvals 251/13, 147/15, and 169/13.

METHOD DETAILS

FRET – ECFP/EYFP experiments were performed using a LSRII flow cytometer instrument (BD Biosciences). EYFP signal was recorded using the 488 nm laser with a 530/30 filter, ECFP signal was recorded using the 405 nm laser with a 450/50 filter and FRET signal was recorded using the 405 nm laser with a 585/42 filter. HEK293T cells were transiently transfected with ECFP and EYFP fusion receptors and analysed 16–20 h post-transfection. Positive FRET cells were gated using an ECFP-EYFP fusion protein as positive control and a co-transfection of ECFP and EYFP as negative control according to (Schneider et al., 2014). EYFP/RFP experiments were performed using a FORTRESSA flow cytometer instrument (BD Biosciences). EYFP signal was recorded using the 488 nm laser with a 530/30 filter, RFP signal was recorded using the 561 nm laser with a 610/20 filter and FRET signals were recorded using the 488 nm laser with a 624/15 filter.

Immunoprecipitations

1×10^6 293T cells transiently transfected with Flag-TACI constructs and untagged or EYFP-tagged constructs were used for immunoprecipitations with anti-Flag resin (Sigma-Aldrich) as described in (Schneider et al., 2014). Immunoprecipitates and input fractions were analysed by SDS-PAGE on 12% acrylamide gels and western blot analysis.

Luciferase reporter assay

HEK293T cells were cultured in 96 well plates at 3×10^5 cells/ml in 100 μ L of medium. After 24 h, cells were transfected with a mix of vectors containing: EGFP (transfection efficiency control) (7 ng), control renilla vector (7 ng), NF- κ B or AP1 firefly luciferase reporter vector (7 ng), various TACI constructs (from 0.05 to 12.8 ng), and full-length BAFF or APRIL (from 0.05 to 12.8 ng), and empty plasmid to reach 70 ng/well of total DNA, using Polyfect transfection reagent (Qiagen). After 24 h, cells were lysed and expression of firefly and renilla luciferases were detected as described (Schneider et al., 2014).

Photo-inducible TACI cross-linking

HEK293T cells were seeded at 2×10^5 cells/ml in a 12 well plate in 1 mL of medium. 24 h later, medium was removed, cells were washed twice with PBS and cultured in 1 mL of leucine/methionine-free medium (DMEM-LM; Thermo Scientific) supplemented with 10% FCS (dialyzed against PBS), 30 mg/mL of L-methionine (Sigma-Aldrich) and 4 mM of L-Photo-Leucine (Thermo Scientific). Transfection was performed 24 h later using JetPrime (Polyplus transfection) according to the manufacturer's protocol. After 24 h of incubation, medium was removed and cells were washed twice with PBS and left in 250 μ L PBS. Cells were exposed for 75 min to UV-light (365 nm), placing the lamp 2 cm on top of the plate (without lid). Whole cell lysates were prepared and analysed by western blot anti-TACI.

Lentiviral gene transfer into primary human B cells

Lentiviral vectors were constructed using the NEBuilder kit of NEB by integrating PCR fragments encoding TACI wildtype or mutant cDNA into pNL-CEF-YFP, a derivative of pNL-CEF-GFP in which GFP was replaced by YFP or RFP (Sic et al., 2014). Naive IgG + CD27- B cells were isolated by depleting other cells using the MojoSort™ Human Naive B Cell Isolation Kit of Biolegend supplemented with biotinylated anti-human CD27 antibodies at 4 μ g/ml (clone O323, Biolegend). Cells were labelled with Cell-Trace Violet (ThermoFisher), plated into U96 wells at 3×10^5 cells/ml, transduced with lentiviral vectors as described before (Kienzler et al., 2013; Pieper et al., 2014) and activated with 0.1 μ M CpG in IMDM containing 10% FCS. After 4 days, cells were isolated and analyzed by flow cytometry.

Knock out in primary human B cells

Naive B cells were isolated from peripheral blood lymphocytes of healthy donors using MACS Naive B-cell Isolation Kit II (Miltenyi Biotec). After isolation, naive B cells were electroporated using the Neon transfection system (Invitrogen, Carlsbad, CA, USA) (1x, 20 ms at 2300 V) with recombinant Cas9-gRNA complexes following manufacturer's instructions (Integrated DNA technologies (IDT), Iowa, USA) and transferred in Iscove's Modified Dulbecco's Medium (IMDM; ThermoFisher, Waltham, MA, USA) supplemented with 20% foetal calf serum (FCS), 100 units/ml penicillin, 100 μ g/ml streptomycin, 1 μ g/ml insulin, 2.5 μ g/ml apo-transferrin, 1% non-essential amino acids, 2 mM glutamine and 1 μ g/ml reduced glutathione as described earlier (Kienzler et al., 2013). After 24 h, cells were rinsed with PBS, 2 mM EDTA and loaded with 1.25 μ M cell trace violet for 20 min at 37°C. Afterwards, cells were washed with IMDM, 10% FCS and resuspended at 1.5×10^6 cell/ml in IMDM, 10% FCS, 50 nM CpG. Cells were incubated at 37°C in 6.6% CO₂ for 3 days. Finally, cells were analysed by flow cytometry.

Molecular modelling

Monte Carlo simulation was performed with Hippo software (Biowerkzeug) using OPLS-AA force field (Kaminski et al., 2001; William L Jorgensen et al., 1996) and generalized born implicit membrane solvation model (J. P. Ulmschneider et al., 2007a; M. B. Ulmschneider et al., 2007b). Distance between C alpha of the c-terminal residue L186 was used to estimate proximity between TM helices along a simulation period of 10^8 steps. All images were generated using PyMOL Molecular Graphics System, Version 1.0, Schrödinger, LLC.

Coarse grained molecular dynamic simulations

The structures of the TM domains of TAC1 (residues 156 to 190), and its variants C172Y and A181E, were constructed as helices using the software PyMOL and then converted to Martini coarse-grain topology using the martinize.py tool (de Jong et al., 2013). The starting system consisted of a box of 25 × 25 × 10 nm with 36 individual CG helices evenly spaced in the XY-plane with their axes oriented in the Z axis as previously described (Sica and Smulski, 2021). The 36 helices were placed in a lipid bilayer on the XY-plane using the INSANE (INSert membrANE) tool, and randomly oriented around Z. The lipids were composed of DOPC and DLPC (7:3) equally distributed on both sides of the membrane. The coarse-grained chain L correlates with 12:0 (lauric) and 14:0 (myristic) saturated fatty acids, whereas chain O correlates with C16:1(9c) (palmitoleic) and C18:1(9c) (oleic) unsaturated fatty acids, allowing to build a model of a biological fluid membrane. The system was completed with CG water beads and consisted of 36 peptides, 1700 lipids, 26000 waters and 600 ions (150 mM concentration), totalling 48000 particles. Simulations were carried out with the GROMCAS package version 2016.5 (Abraham et al., 2015) using the Martini v2.1 forcefield (Marrink et al., 2007). After the initial steps of minimization and equilibration the systems were simulated with a 20 fs time step at 310 K and 1 bar using the velocity rescaling thermostat of Bussi et al. (Bussi et al., 2007) and the semi-isotropic Parrinello-Rahman barostat. Every system was simulated for at least 7 μs.

Radial density

First, the centroid (C) of every helix was computed between a defined central backbone (BB) atom (i) and two consecutive BB atom at each side in the sequence $C_i = (r_{i-2} + r_{i-1} + r_i + r_{i+1} + r_{i+2})/5$, where r is the XYZ-coordinate of the atom. Second, the unit bisection vector was computed between the central (i) and adjacent BB atoms (i±1), according to the method of Khan to identify the helix orientation (Kahn, 2001). Third, a reference frame was defined with the centroid of the reference helix as origin and its orientation vector as unit X-vector, and the position of the centroids of the remaining 35 helices were computed. This procedure was repeated for all 36 helices present in the membrane patch along the indicated simulation time every 100 ns until the end of the simulated period. The scatter plot of the accumulated XY-centroids positions was transformed to a density map with ggplot implemented in R.

Contact maps

For each residue (i) of every helix (H) the number of contacts against all the other residues in the remaining helices, along the simulation time (T) was computed. A contact was defined when the BB atoms of two residues are located at XYZ-distance equal to or less than an arbitrary cut-off, as follows:

$$C_{ij}^{KL} = \begin{cases} 1, & \text{if } \|r_i^K - r_j^H\| \leq d_{\text{cutoff}} \\ 0, & \text{if } \|r_i^K - r_j^H\| > d_{\text{cutoff}} \end{cases}$$

where i and j are the residue number in the peptide sequence ($i = \{1, \dots, j, \dots, N\}$), and H and K are the helices analysed ($H = \{1, \dots, K, \dots, 36\}$). Thus, the number of contacts (NC) for every residue i against each residue j in the remaining (K) helices were computed as:

$$NC_{ij} = \sum_T \sum_j^{K \neq H} C_{ij}^{HK}$$

QUANTIFICATION AND STATISTICAL ANALYSIS

EYFP-EYFP FRET experiments (Figure S3) and gRNA comparison (Figures 6B, 6D, 6E and S6B) were analysed using one-way ANOVA with Tukey's multiple comparisons test. Proliferation (Figure 5C) and IgA class switch (Figure 5D) were analysed with one-way Brown-Forsythe and Welch ANOVA test (not assuming equal standard deviations), with Dunnett T3 multiple comparison test. EYFP-RFP FRET experiments ± BAFF (Figures 3D–3G) were analysed using two-way ANOVA with Tukey's multiple comparisons test. Statistical analysis was performed using GraphPad Prism version 9.3.1 for Mac OS X, GraphPad Software, San Diego California USA, www.graphpad.com (ns p > 0.05).

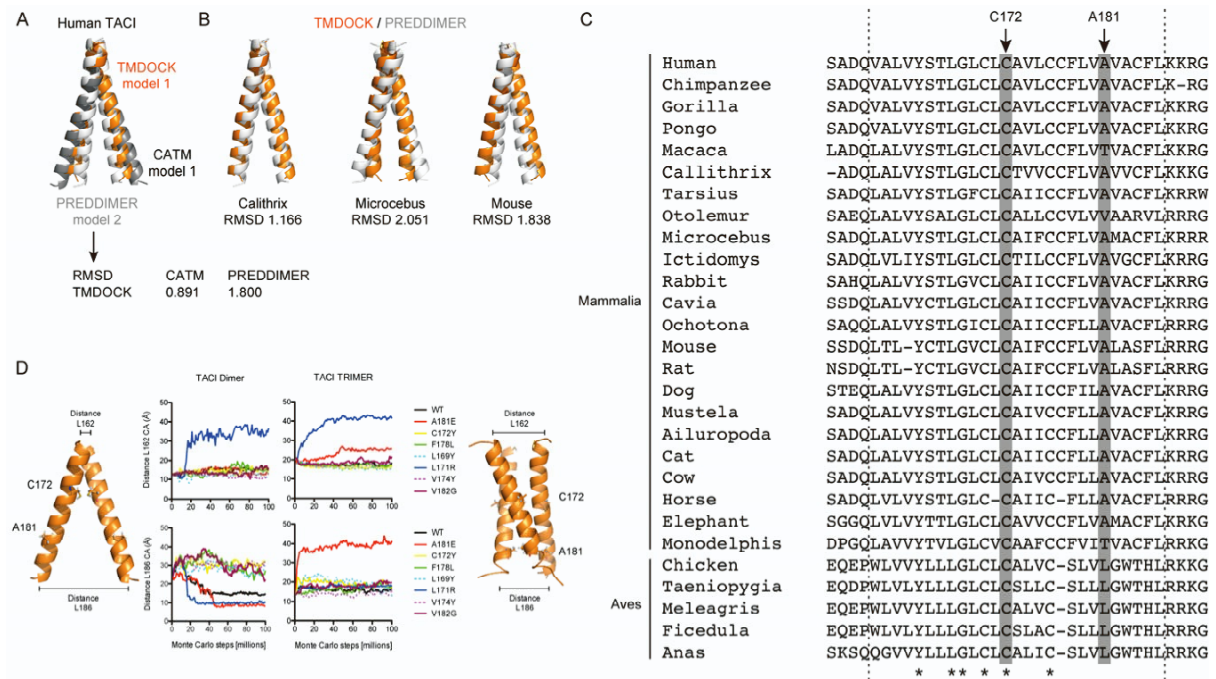
Supplemental information

**Ligand-independent oligomerization
of TACI is controlled by the transmembrane domain
and regulates proliferation of activated B cells**

Cristian R. Smulski, Luyao Zhang, Malte Burek, Ariadna Teixidó Rubio, Jana-Susann Briem, Mauricio P. Sica, Eirini Sevdali, Michele Vigolo, Laure Willen, Patricia Odermatt, Duygu Istanbulu, Stephanie Herr, Marco Cavallari, Henry Hess, Marta Rizzi, Hermann Eibel, and Pascal Schneider

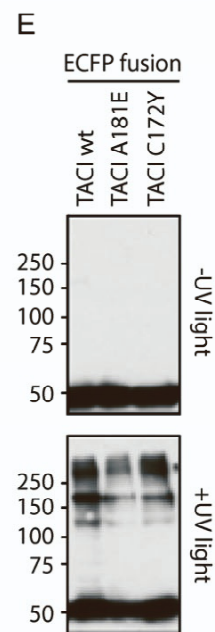
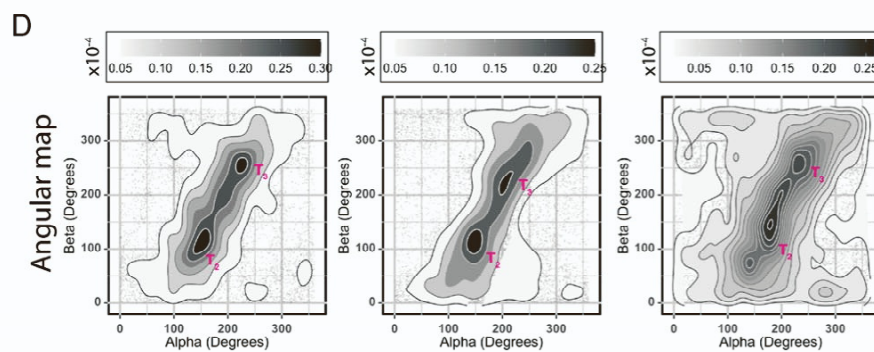
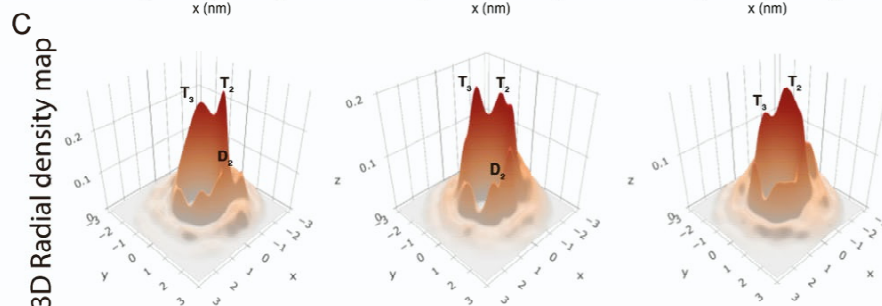
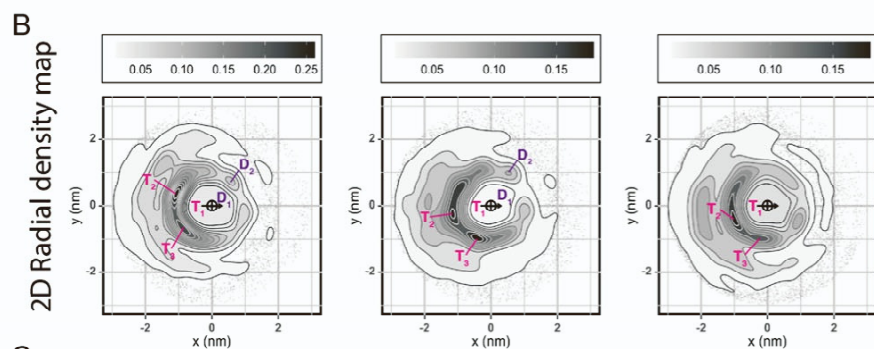
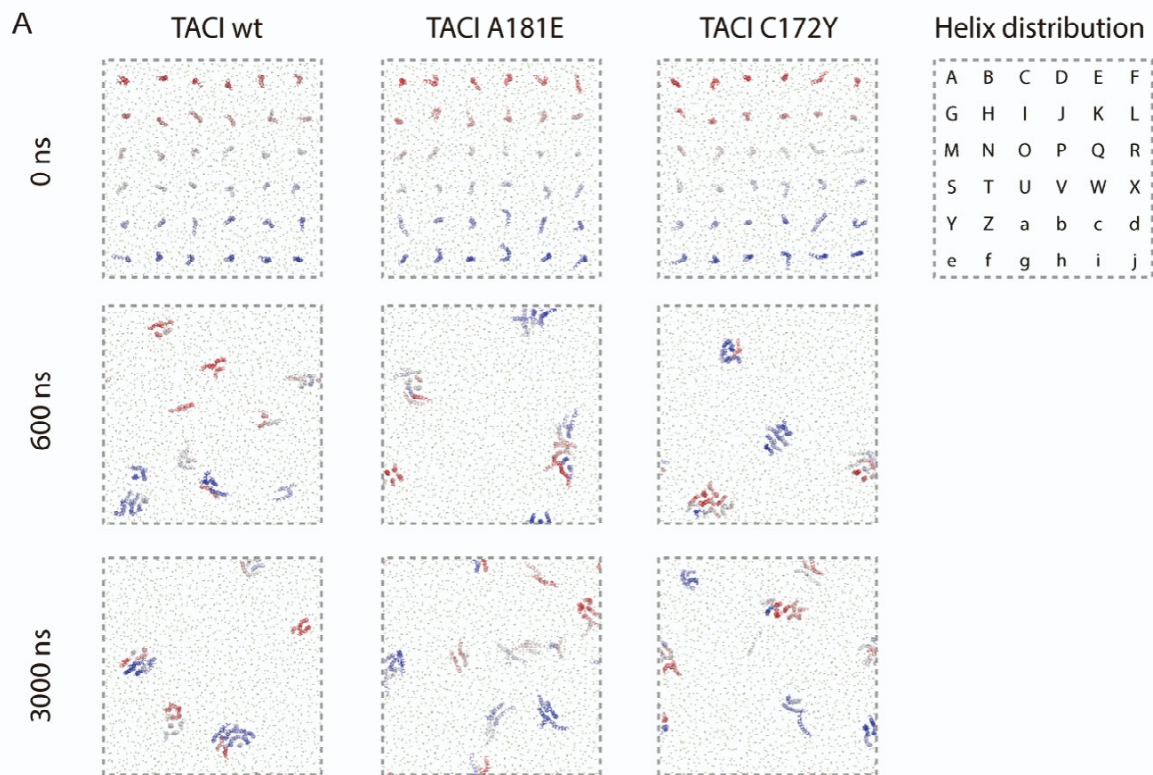
Supplemental information for manuscript

“Ligand-independent oligomerization of TACI is controlled by the transmembrane domain and regulates proliferation of activated B cells.”



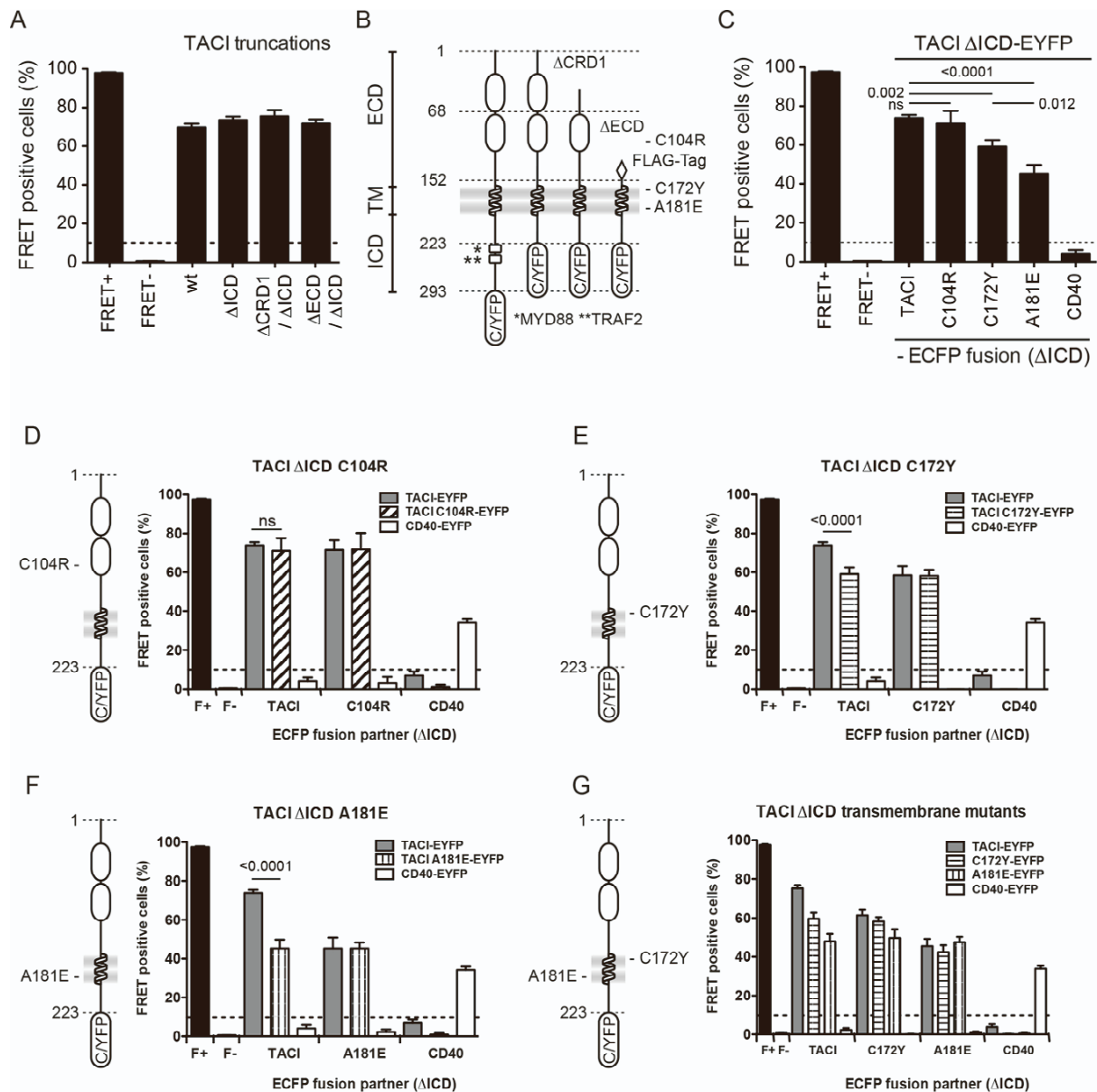
Supplemental figure 1 (related to figure 1). TACI transmembrane assembly model.

A. Superposition of the top scored dimeric assembly models of TACI transmembrane region. TMDOCK model 1 (orange), CATM model 1 (black) and PREDDIMER model 2 (grey). The root mean square deviations (RMSD) between these three structures are indicated at the bottom and indicate high similarities between models. **B.** Superimposition of dimeric structures of TACI transmembrane domain obtained by TMDOCK (orange) and PREDDIMER (grey) for three randomly chosen mammals. **C.** Sequence alignment of TACI transmembrane sequence of several mammals and birds. The positions C172 and A181 are shaded in grey. Fully conserved residues are indicated with (*) at the bottom of the alignment. **D.** Monte Carlo simulation of the impact of different TACI TM variants (A181E, C172Y, F178L, L171R, V182G) annotated in the ClinVar database (NCBI) or rationally designed variants (L169Y, V174Y) on the dimeric and trimeric assembly.



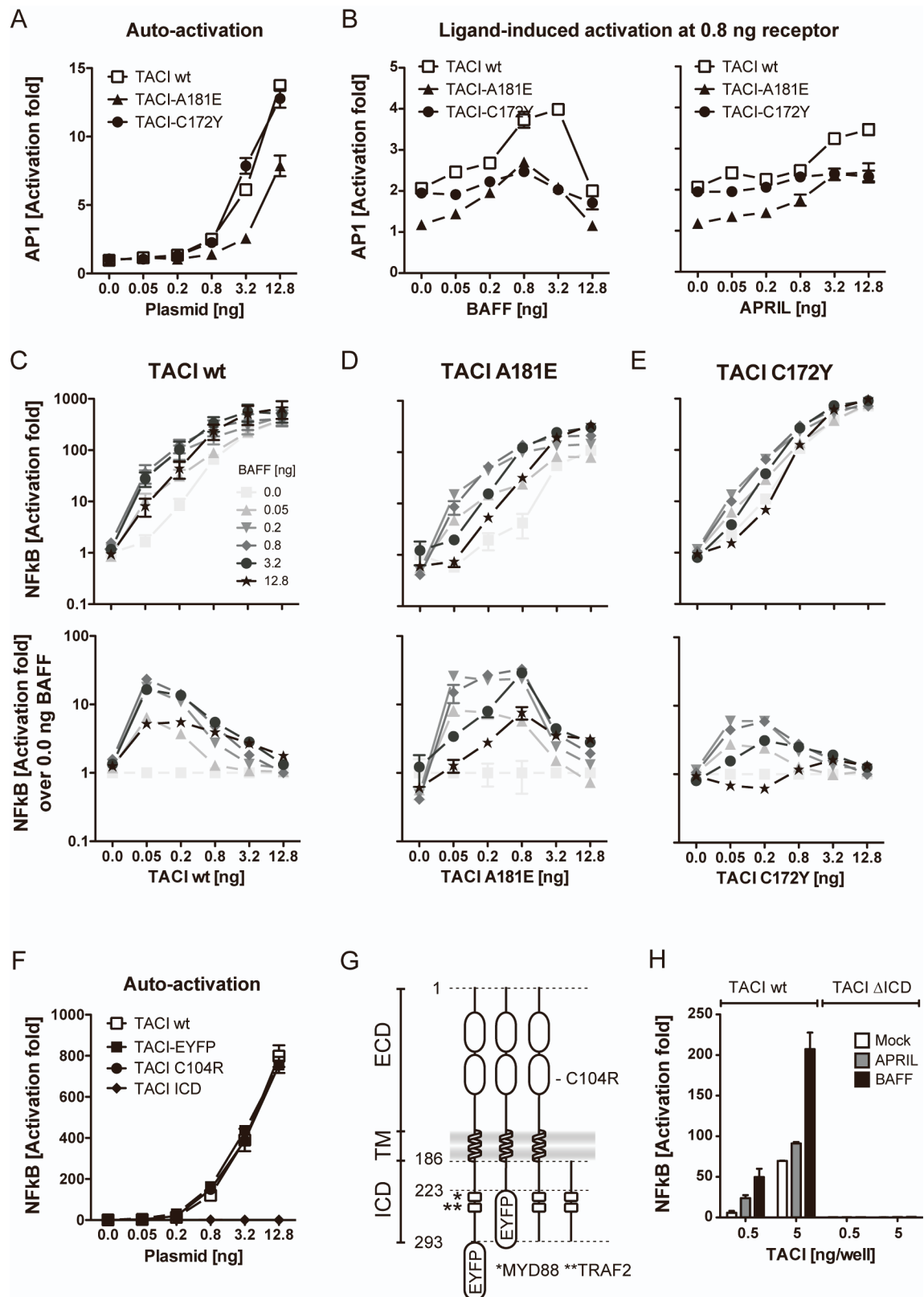
Supplemental figure 2 (related to figure 2). TACI transmembrane domain organizes mainly as trimers through the A181 interface in simulated membranes.

A. Coarse-grain molecular dynamic simulation of 36 TACI transmembrane domains, wild type (wt) or with mutations A181E or C172Y embedded in a membrane formed of coarse-grained models of DOPC and DLPC (7:3) equally distributed on both sides of the membrane. Snapshots were taken at 0, 600 and 3000 ns. Helix distribution in the membrane is illustrated on the right. **B.** The most frequent organization in the XY plane is observed in the radial density maps (2D) where the position of each helix against the remaining 35 ones is computed all along the simulated period and superimposed at the centre of the quadrant. The centre of reference and orientations vectors were determined as illustrated in figure 2A. For the trimeric assembly, the most dense positions are indicated as T₂ and T₃ (T₁ being the centre of the reference helix). For the dimeric assembly, the most dense position is indicated as D₂ (D₁ being the centre of the reference helix). **C.** 3D version of the radial density map shown in panel (B). **D.** Angular map for the different TACI variants showing the preferred relative orientation (beta) for each position around the central helix (alpha). The orientations vectors were determined as illustrated in figure 2C. Scales in panels B and C correspond to the 2D kernel density estimation. **E.** Crosslinking of TACI WT, A181E and C172Y fused to EYFP in HEK 293T cells labelled with a photo-activatable leucine analogue. Whole cell extracts were analysed by western blotting using anti-GFP antibodies that recognize EYFP fused to TACI.



Supplemental figure 3 (related to figure 3). Oligomerization and interactions of TACI polypeptide chains.

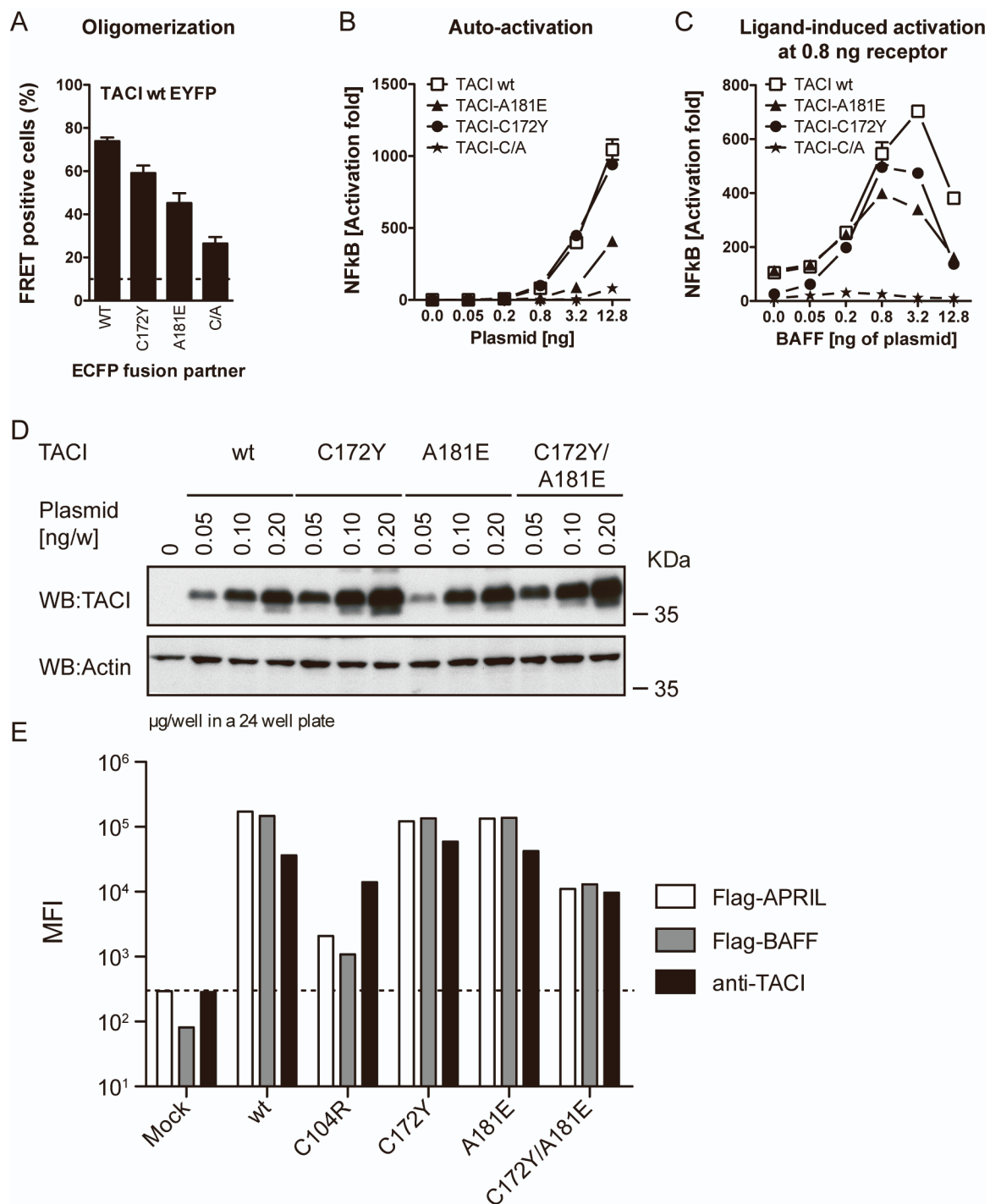
A. Oligomerization analysis by Förster Resonance Energy Transfer (FRET) of TACI truncations schematized in panel (B). In all panels FRET+ corresponds to an EYFP-ECFP fusion protein, while FRET- corresponds to the co-transfection of EYFP and ECFP. At least 9 independent experiments were averaged for each truncation. **B.** Scheme of the different TACI truncations used in this figure. TACI Δ CRD1 (1-223 Δ 21-67 \rightarrow W) corresponds to TACI-S (isoform 2). **C.** FRET analysis of wt TACI Δ ICD-EYFP with wt TACI, C104R, C172Y or A181E Δ ICD-ECFP. CD40 Δ ICD-ECFP was used as a negative control. At least 5 independent experiments were averaged for each pair. **D.** FRET analysis of TACI wt and C104R, both Δ ICD. **E.** FRET analysis of TACI wt and C172Y, both Δ ICD. **F.** FRET analysis of TACI wt and A181E, both Δ ICD. **G.** FRET analysis of TACI wt, C172Y and A181E - Δ ICD in all combinations. CD40 was used as a negative control.



Supplemental figure 4 (related to figure 4). TACI transmembrane domain regulates ligand-independent and ligand-dependent activation.

A. AP1-luciferase reporter assay after transfection of the indicated amounts of plasmids for TACI wt, C172Y or A181E in the absence of ligand (auto-activation). **B.** AP1-luciferase reporter

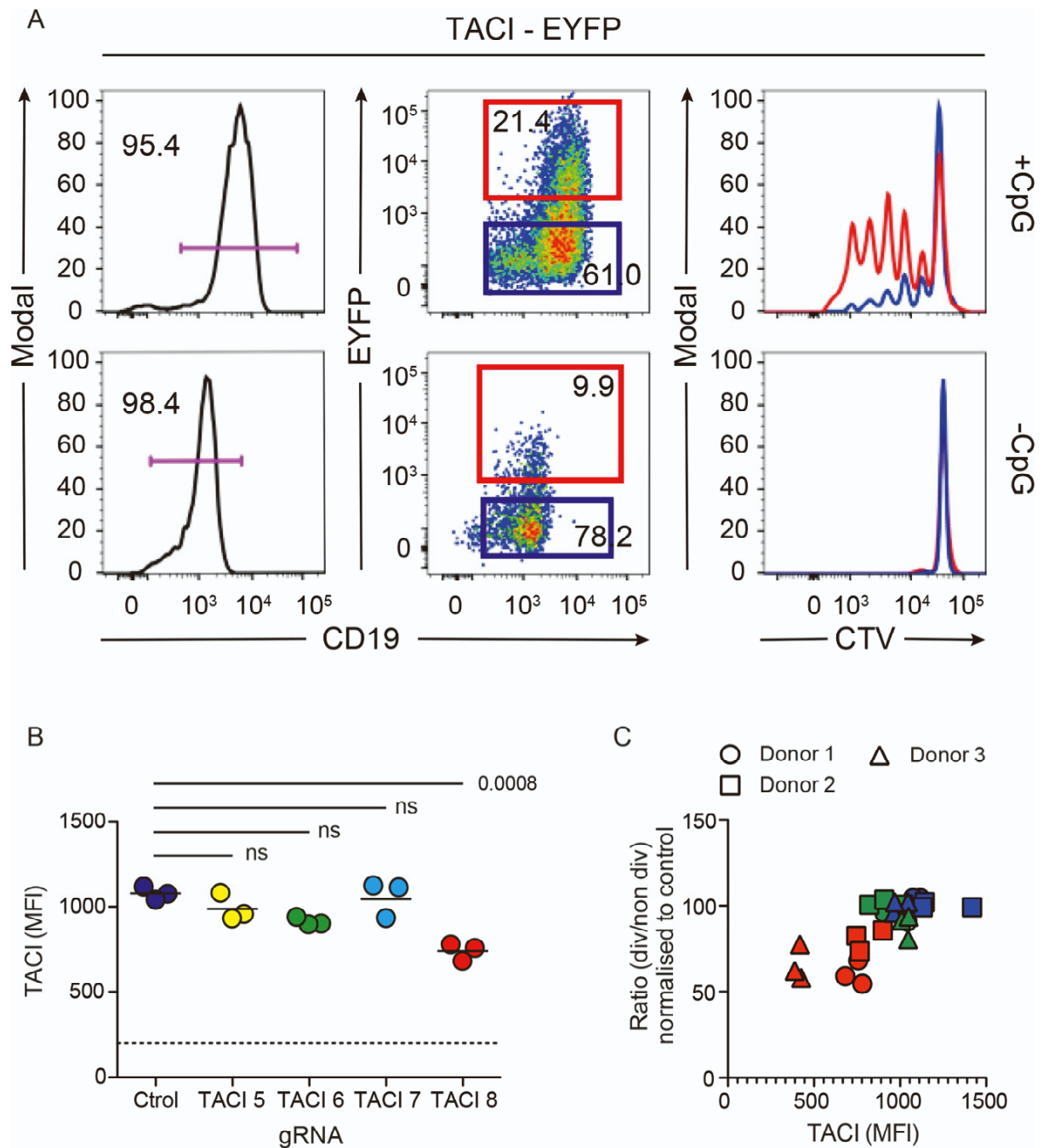
assay after transfection of 0.8 ng of TACI wt, A181E or C172Y with the indicated amounts of APRIL (left) or BAFF (right) plasmid. **C-E.** Activation of a NF κ B-luciferase reporter with the indicated amounts of TACI wt, A181E or C172Y plasmids and variable amounts of BAFF plasmid, normalized to a condition without TACI and BAFF. Bottom panels show ligand-dependent activation only, calculated as a ratio to the no-ligand condition (auto-activation) for each receptor concentration used. **F.** NF κ B-luciferase reporter assay after transfection of the indicated amounts of plasmids for full length wt TACI, full length TACI fused to EYFP, TACI C104R and TACI intracellular domain (ICD) in the absence of ligand (auto-activation). **G.** Scheme of the plasmids used in panels (F and H). **H.** NF κ B-luciferase reporter assay after transfection of the indicated amounts of plasmids coding for wt TACI (full-length) and TACI Δ ICD (lacking the TRAF binding site). The assay was performed in the absence of ligand (Mock) or with co-transfection of 5 ng/well of APRIL- or BAFF-coding plasmids.



Supplemental figure 5 (related to figures 4 and S4). TACI transmembrane domain regulates ligand-independent and ligand-dependent activation.

A. Oligomerization analysis by Forster Resonance Energy Transfer (FRET) of EYFP-fused TACI 1-223 in combination with ECFP-fused TACI wt, C172Y, A181E and the double mutant C172Y/A181E, all Δ ICD. **B.** NFkB-Luciferase reporter assay titrating the indicated amounts of TACI wt, C172Y, A181E and the double mutant C172Y/A181E in the absence of ligand (auto-activation). **C.** NFkB-Luciferase reporter assay titrating the indicated amounts of BAFF on a single concentration (0.8 ng) of TACI wt, C172Y, A181E and the double mutant C172Y/A181E

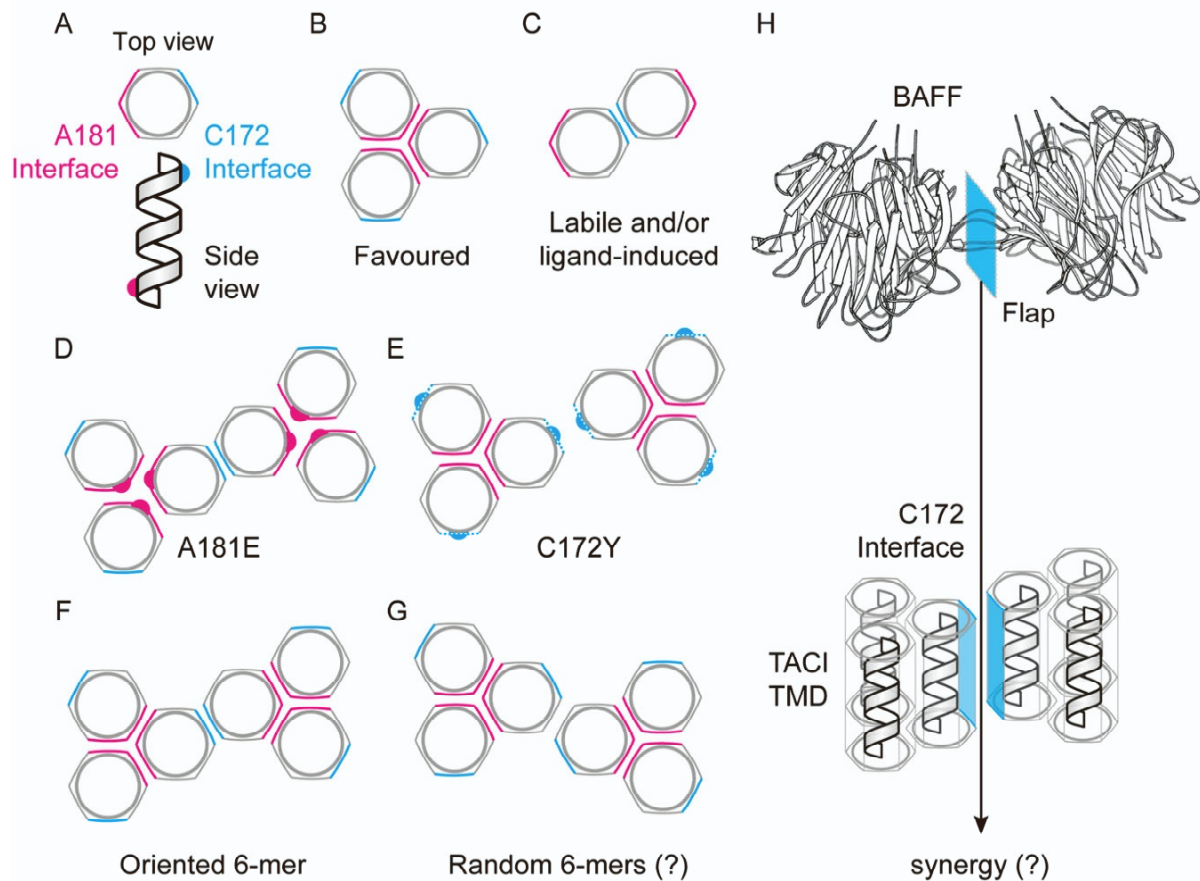
(ligand-induced activation). **D.** Western blot analysis of TACI wt, C172Y, A181E and C172Y/A181E expression levels at the indicated concentrations. **E.** Flow cytometry detection of untagged TACI wt, C104R, C172Y, A181E and C172Y/A181E by an anti-TACI antibody or by Flag-BAFF or Flag-APRIL.



Supplemental figure 6 (related to figures 5 and 6). Overexpression of TACI does not induce cell division.

A. IgD⁻ CD27⁻ B cells were isolated by magnetic depletion of all other cells, labelled with cell trace violet (CTV) and transduced with a lentiviral vector encoding TACI-YFP. Cells were then either activated with 0.1 μ M CpG (top row) or not (bottom row), cultivated for 4 days at 37°C and analysed by flow cytometry. The histogram overlays (right column) show CD19⁺ cells (left column) gated for TACI-YFP expression into YFP⁺ and YFP⁻ cells. **B.** Mean fluorescence intensity (MFI) TACI expressed by B cells electroporated with a mock (Cas9/enhancer mix, control) or with four different TACI gRNA/Cas9 complexes. Dotted line corresponds to isotype control MFI levels. **C.** Correlation between TACI expression levels and the ratio

proliferating/non-proliferating cells, following CRISPR/Cas9 inactivation of TACI in CpG activated primary B cells. Pearson correlation test $p < 0.0001$.



Supplemental figure 7 (related to figures 1 to 6). Working model of the implication of TACI transmembrane domain in signalling.

A. Representation of a single TACI TM helix, top and side views. The dimeric interaction interface C172 is represented in cyan, and the trimeric interaction interface A181 in magenta. **B.** The favoured trimeric assembly of TACI TM region is mediated by the A181 interface. **C.** A labile and/or ligand-induced dimeric assembly of TACI TM region is mediated by the C172 interface. **D.** Mutation A181E affects but does not disrupt trimeric assembly. The C172 interface is not much impaired. **E.** Mutation C172Y disturbs dimeric interactions, and also affects trimeric interactions to some extent. **F.** Hexameric conformation of TACI TM region “oriented” via the C172 interface that would occur during ligand-dependent signalling. **G.** Hypothetic “random” hexameric conformation(s) of TACI TM region that may form during ligand-independent signalling. **H.** Model for ligand-induced oligomerization of TACI TM region. Weak FLAP interactions in BAFF and weak TACI interactions at the C172 interface may possibly stabilize each other to promote ligand-dependent signalling.

Table S1 (related to figures 6 and S6): TACI gRNA sequences:

Name	IDT-ID	Sequence	PAM
TACI 5	Hs.Cas9.TNFRSF13B.1.AA	CTCGGGAAGGTACCAAGGAT	TGG
TACI 6	Hs.Cas9.TNFRSF13B.1.AB	TCATAGCCACCCCGTCCAC	AGG
TACI 7	Hs.Cas9.TNFRSF13B.1.AC	GTTCTATGACCATCTCCTGA	GGG
TACI 8	Hs.Cas9.TNFRSF13B.1.AL	ACAATTCAGACAACCTCGGGA	AGG

IDT: Integrated DNA technologies (Iowa, USA).

Table S2 (related to figures 1, 3, 4, 5, S2, S3, S4 and S5): List and description of the plasmids used in the study.

Plasmid	Designation	Protein encoded	Backbone
ps015	Empty	Empty	PCR3
ps2155	EYFP	EYFP (1-239)	PCR3
ps2156	ECFP	ECFP (1-239)	PCR3
ps2565	His6-hBAFF	MRGSHHHHHHS-h BAFF (134-285)	pQE9
ps2967	EYFP-ECFP	EYFP (1-239)-GGIETDGSIEDGG-ECFP (1-239)	pcDNA3.1 zeo
ps2460	hCD40 1-260-EYFP	hCD40 (1-260)-VDEFPVAT-EYFP (1-239)	PCR3
ps2461	hCD40 1-260-ECFP	hCD40 (1-260)-VDEFPVAT-ECFP (1-239)	PCR3
ps3260	hTACI 1-293-EYFP	hTACI (1-293)-EFPVAT-EYFP (1-239)	PCR3
ps3285	hTACI 1-293-ECFP	hTACI (1-293)-EFPVAT-ECFP (1-239)	PCR3
ps2252	hTACI 1-223-EYFP	hTACI (1-223)-EFPVAT-EYFP (1-239)	PCR3
ps2253	hTACI 1-223-ECFP	hTACI (1-223)-EFPVAT-ECFP (1-239)	PCR3
ps3281	hTACI 1-20 W 68-223-EYFP	hTACI (1-20)-W-(68-223)-EFPVAT-EYFP (1-239)	PCR3
ps3282	hTACI 1-20 W 68-223-ECFP	hTACI (1-20)-W-(68-223)-EFPVAT-ECFP (1-239)	PCR3
ps3250	Flag-hTACI 152-223-EYFP	HA signal-Flag-GPGQVQLQ-hTACI (152-223)-EFPVAT-EYFP (1-239)	PCR3
ps3242	Flag-hTACI 152-223-ECFP	HA signal-Flag-GPGQVQLQVD-hTACI (152-223)-EFPVAT-ECFP (1-239)	PCR3
ps2258	hTACI 1-223 C104R-EYFP	hTACI (1-223, C104R)-EFPVAT-EYFP (1-239)	PCR3
ps2259	hTACI 1-223 C104R-ECFP	hTACI (1-223, C104R)-EFPVAT-ECFP (1-239)	PCR3
ps3289	hTACI 1-223 C172Y-EYFP	hTACI (1-223, C172Y)-EFPVAT-EYFP (1-239)	PCR3
ps3291	hTACI 1-223 C172Y-ECFP	hTACI (1-223, C172Y)-EFPVAT-ECFP (1-239)	PCR3
ps2254	hTACI 1-223 A181E-EYFP	hTACI (1-223, A181E)-EFPVAT-EYFP (1-239)	PCR3
ps2255	hTACI 1-223 A181E-ECFP	hTACI (1-223, A181E)-EFPVAT-ECFP (1-239)	PCR3
ps4245	hTACI 1-293-EYFP	hTACI (1-293)-GPVAT-EYFP (1-239)	pNL-CEF
ps4246	hTACI 1-293-RFP	hTACI (1-293)-GGSGSDPPVAT-RFP (1-237)	pNL-CEF
ps4272	hTACI 1-21 68-223-EYFP	hTACI (1-21)-(68-223)-GPVAT-EYFP (1-239)	pNL-CEF
ps4248	hTACI 1-21 68-223-RFP	hTACI (1-21)-(68-223)-GGSGSDPPVAT-RFP (1-237)	pNL-CEF
ps4249	hTACI 1-293-EYFP A181E	hTACI (1-293 A181E)-GPVAT-EYFP (1-239)	pNL-CEF
ps4250	hTACI 1-293-RFP A181E	hTACI (1-293 A181E)-GGSGSDPPVAT-RFP (1-237)	pNL-CEF
ps4251	hTACI 1-293-EYFP C172Y	hTACI (1-293 C172Y)-GPVAT-EYFP (1-239)	pNL-CEF
ps4252	hTACI 1-293-RFP C172Y	hTACI (1-293 C172Y)-GGSGSDPPVAT-RFP (1-237)	pNL-CEF
ps4253	hTACI 1-293-EYFP C104R	hTACI (1-293 C104R)-GPVAT-EYFP (1-239)	pNL-CEF
ps4254	hTACI 1-293-RFP C104R	hTACI (1-293 C104R)-GGSGSDPPVAT-RFP (1-237)	pNL-CEF

ps4255	hTACI 152-293-EYFP	HA signal-Flag-GPGQVQLQVD-(152-293)-EFPVAT-EYFP (1-239)	pNL-CEF
ps4256	hTACI 152-293-RFP	HA signal-Flag-GPGQVQLQVD-(152-293)-GGSGSDPPVAT-RFP (1-237)	pNL-CEF
ps4257	hCD40 1-260-EYFP	hCD40 (1-277)-DPVAT-EYFP (1-239)	pNL-CEF
ps4258	hCD40 1-260-RFP	hCD40 (1-277)-DGSAGSDPPVAT-RFP (1-237)	pNL-CEF
ps4259	hTACI 1-223-EYFP	hTACI (1-223)-EFPVAT-EYFP (1-239)	pNL-CEF
ps2595	Flag-hTACI	HA signal-Flag-GPGQVQLQVD-hTACI (2-293)	PCR3
ps2596	VSV-hTACI	HA signal-VSV-GPGQVQLQVD-hTACI (2-293)	PCR3
ps863	VSV-hBCMA	HA signal-VSV-GPGQVQLQ-hBCMA (2-184)	PCR3
ps2165	AP1 luciferase		pGL3
ps1614	NFκB luciferase		Other
ps1615	Renilla		Other
ps515	EGFP	EGFP (1-239)	pcDNA3.1 zeo
ps1383	hTACI	hTACI (1-293)	PCR3
ps2154	hTACI C104R	hTACI (1-293, C104R)	PCR3
ps2172	hTACI C172Y	hTACI (1-293, C172Y)	PCR3
ps2153	hTACI A181E	hTACI (1-293, A181E)	PCR3
ps1861	hAPRIL	hAPRIL (1-250)	PCR3
ps544	hBAFF	hBAFF (1-285)	PCR3
ps3709	Flag-hTACI 152-293-EYFP	HA signal-Flag-GPGQVQLQVD-hTACI (152-293)-EFPVAT-EYFP (1-239)	PCR3
ps3705	Flag-hTACI 152-293 A181E-EYFP	HA signal-Flag-GPGQVQLQVD-hTACI A181E (152-293)-EFPVAT-EYFP (1-239)	PCR3
ps3731	Flag-hTACI 152-293 C172Y-EYFP	HA signal-Flag-GPGQVQLQVD-hTACI C172Y (152-293)-EFPVAT-EYFP (1-239)	PCR3
ps3704	hTACI 1-20 W 68-293-EYFP	hTACI (1-20)-W-(68-293)-EYFP (1-239)	PCR3
ps1301	VSV-hTACI ICD	MY-VSV-EF-hTACI (187-293)	PCR3

HA signal=MAIYLILLFTAVRG Flag=DYKDDDDK VSV=TDIEMNRLGK

Plasmid maps and primary data for all graphs are available at DOI 10.5281/zenodo.6122280